

# The University of British Columbia

Faculty of Graduate Studies



PROGRAMME OF THE  
FINAL ORAL EXAMINATION  
FOR THE DEGREE OF  
DOCTOR OF PHILOSOPHY

*of*

**MAX LYNN SWANSON**

B. A. University of British Columbia

M. Sc. University of British Columbia

**IN ROOM 204, PHYSICAL METALLURGY BUILDING**

**MONDAY, MAY 5, 1958, at 10:30 a. m.**

**COMMITTEE IN CHARGE**

**DEAN G. M. SHRUM, *Chairman***

**W. M. ARMSTRONG**

**B. SAVERY**

**F. A. FORWARD**

**W. O. RICHMOND**

**E. TEGHTSOONIAN**

**C. A. McDOWELL**

**B. MOYLES**

**R. W. STEWART**

External Examiner: **B. N. BROCKHOUSE**  
Chalk River Ont.

## **THE CONSTRUCTION OF AN ADIABATIC CALORIMETER AND ITS USE IN MEASURING SPECIFIC HEATS**

### **A B S T R A C T**

A fluidless adiabatic calorimeter was constructed and was used to measure the specific heats of manganese-aluminum-carbon and manganese-zinc-carbon alloys from  $-150^{\circ}$  to  $150^{\circ}\text{C}$ .

In an adiabatic calorimeter, the temperature of a shield surrounding the calorimeter vessel is kept at approximately the same temperature as that of the vessel, so that the thermal leakage between the two is reduced to a negligible quantity. Thus the ordinary rating period, in which the thermal leakage modulus is calculated, can be eliminated. Since leakage modulus variations are reduced by the adiabatic method, it can be used for large temperature rises, resulting in fast and accurate measurements. The aneroid (fluidless) adiabatic calorimeter eliminates stirring and evaporation errors, and makes possible measurements at extreme temperatures.

The calorimeter consisted of a cylindrical silver-plated copper vessel surrounded by an electrically heated adiabatic shield and an evacuated outer case. A platinum resistance thermometer-heater was used to supply heat to the calorimeter vessel and to measure the vessel temperature. The heat input and the thermometer resistance were measured by using a potentiometer in conjunction with standard resistances.

The thermometer was calibrated by measuring its resistance at  $-183$ ,  $-40$ ,  $0$ , and  $100^{\circ}\text{C}$ . The calorimeter was calibrated from  $-150$  to  $150^{\circ}\text{C}$ . The accuracy of the calorimeter was approximately 0.5%, the main error arising from the method of measuring the temperature of the calorimeter vessel.

The specific heat curves of the single phase magnetic alloys  $Mn_3AlC$  and  $Mn_3ZnC$  were measured. A second order specific heat anomaly was found, as expected, for the ferromagnetic alloy  $Mn_3AlC$  at its Curie point,  $-10^\circ C$ . Although the anomaly was close to the theoretical shape, dropping to zero over only a  $10^\circ C$  range at the Curie point, its maximum height was less than saturation magnetization measurements would indicate.

The alloy  $Mn_3ZnC$  showed second order specific heat anomalies at  $-35^\circ C$ , and at  $65^\circ C$ . This double specific heat anomaly indicates, in agreement with neutron diffraction results, a complex magnetic behavior for the alloy. Although the high temperature Curie point anomaly did not have a sharp peak the low temperature anomaly's shape approached that of the theoretical Weiss curve.

## GRADUATE STUDIES

### Field of Study: Metallurgy (Metal Physics)

Structure of Metals .....	W. Armstrong
Phase Transformations in Metals .....	W. Armstrong
Ferromagnetism .....	H. Meyers
Plastic Deformations and Lattice Imperfections	H. Meyer
Bonding in Metals .....	J. Halpern
X-Ray Diffraction .....	J. Parr

### Other Studies:

Theory of Measurements .....	W. Opechowski
Quantum Mechanics .....	G. M. Volkoff
Electromagnetic Theory .....	J. Brown
Nuclear Physics .....	K. Mann
Chemical Physics .....	C. Reid
Group Theory .....	B. Moyls

THE CONSTRUCTION OF AN ADIABATIC CALORIMETER  
AND ITS USE IN MEASURING SPECIFIC HEATS

by

MAX SWANSON

A THESIS SUBMITTED IN PARTIAL FULFILMENT OF  
THE REQUIREMENTS FOR THE DEGREE OF  
DOCTOR OF PHILOSOPHY

in the Department

of

MINING AND METALLURGY

We accept this thesis as conforming to the  
standard required from candidates for the  
degree of DOCTOR OF PHILOSOPHY.

Members of the Department of  
Mining and Metallurgy.

The University of British Columbia

December 1957.

## ABSTRACT

A fluidless adiabatic calorimeter was constructed and was used to measure the specific heats of manganese-aluminum-carbon and manganese-zinc-carbon alloys from  $-150^{\circ}$  to  $150^{\circ}\text{C}$ .

In an adiabatic calorimeter, the temperature of a shield surrounding the calorimeter vessel is kept at approximately the same temperature as that of the vessel, so that the thermal leakage between the two is reduced to a negligible quantity. Thus the ordinary rating period, in which the thermal leakage modulus is calculated, can be eliminated. Since leakage modulus variations are reduced by the adiabatic method, it can be used for large temperature rises, resulting in fast and accurate measurements. The aneroid (fluidless) adiabatic calorimeter eliminates stirring and evaporation errors, and makes possible measurements at extreme temperatures.

The calorimeter consisted of a cylindrical silver-plated copper vessel surrounded by an electrically heated adiabatic shield and an evacuated outer case. A platinum resistance thermometer-heater was used to supply heat to the calorimeter vessel and to measure the vessel temperature. The heat input and the thermometer resistance were measured by using a potentiometer in conjunction with standard resistances.

The thermometer was calibrated by measuring its resistance at  $-183$ ,  $-40$ ,  $0$ , and  $100^{\circ}\text{C}$ . The calorimeter was calibrated from  $-150$  to  $150^{\circ}\text{C}$ . The accuracy of the calorimeter was approximately 0.5%, the main error arising from the method of measuring the temperature of the calorimeter vessel.

The specific heat curves of the single phase magnetic alloys  $\text{Mn}_3\text{AlC}$  and  $\text{Mn}_3\text{ZnC}$  were measured. A second order specific heat anomaly was found, as

expected, for the ferromagnetic alloy  $Mn_3AlC$  at its Curie point,  $-10^\circ C$ . Although the anomaly was close to the theoretical shape, dropping to zero over only a  $10^\circ C$  range at the Curie point, its maximum height was less than saturation magnetization measurements would indicate.

The alloy  $Mn_3ZnC$  showed second order specific heat anomalies at  $-35^\circ C$ , and at  $65^\circ C$ . This double specific heat anomaly indicates, in agreement with neutron diffraction results, a complex magnetic behaviour for the alloy. Although the high temperature Curie point anomaly did not have a sharp peak, the low temperature anomaly's shape approached that of the theoretical Weiss curve.

In presenting this thesis in partial fulfilment of the requirements for an advanced degree at the University of British Columbia, I agree that the Library shall make it freely available for reference and study. I further agree that permission for extensive copying of this thesis for scholarly purposes may be granted by the Head of my Department or by his representative. It is understood that copying or publication of this thesis for financial gain shall not be allowed without my written permission.

Department of Metallurgy

The University of British Columbia,  
Vancouver 8, Canada.

Date May 7, 1958

## ACKNOWLEDGEMENTS

The author is grateful for the advice and technical assistance given by his research director, Dr. H.P. Myers, and by R. Butters and R. Richter. He would also like to thank L. Howe for his preliminary reading of the thesis.

The work was carried out with the help of Research Grant 281 provided by the Defence Research Board, and a Studentship from the National Research Council.

## TABLE OF CONTENTS

	<u>Page</u>
I. INTRODUCTION .....	1
1. Specific Heat Theory .....	1
2. The Alloys to be Investigated .....	6
3. Calorimetric Theory .....	12
II. THE CONSTRUCTION OF AN ANEROID ADIABATIC CALORIMETER ....	17
1. Design .....	17
2. Materials and Detailed Construction .....	19
III. CALIBRATION AND PERFORMANCE .....	34
1. Calibration of Resistance Thermometer .....	34
2. Heat Capacity of the Calorimeter .....	42
3. Accuracy of Specific Heat Measurements .....	42
IV. RESULTS .....	52
1. Preparation and Properties of Alloys .....	52
2. Specific Heat Measurements .....	56
V. DISCUSSION AND CONCLUSIONS .....	68
1. Discussion of Results .....	68
2. Conclusions .....	68k
VI. APPENDICES .....	69
VII. BIBLIOGRAPHY .....	84

## FIGURE INDEX

	<u>Page</u>
1. Perovskite Structure . . . . .	7
2. Variation of Saturation Magnetization, $\sigma$ , with Temperature, T, for Mn-Zn-O Alloys . . . . .	10
3. Possible Magnetic Structure at 0°K of Mn <sub>3</sub> ZnC . . . . .	11
4. Basic Calorimeter Design . . . . .	18
5. The Calorimeter . . . . .	21
6. Adiabatic Shield Control Circuit . . . . .	24
7. Suspension of the Calorimeter . . . . .	27
8. Circuit Diagrams for Thermometer-Heaters . . . . .	31
9. Calibration Apparatus . . . . .	37
10. Heat Capacities of Calorimeter and of Calorimeter plus Alumina . . . . .	44
11. Variation of Thermal Leakage Modulus, k, with Pressure . . . . .	47
12. The Variation of Saturation Magnetization, $\sigma$ , with Temperature, T, for Mn <sub>3</sub> AlC . . . . .	54
13. The Variation of Saturation Magnetization, $\sigma$ , with Temperature, T, for Mn <sub>3</sub> ZnC . . . . .	55
14. Capacity of Mn <sub>3</sub> AlC plus Calorimeter . . . . .	58
15. Capacity of Mn <sub>3</sub> AlC . . . . .	59
16. Capacity of Mn <sub>3</sub> AlC plus Calorimeter (using the strain-free thermometer) . . . . .	60
17. Capacity of Mn <sub>3</sub> ZnC (alloy 1) plus Calorimeter . . . . .	62
18. Capacity of Mn <sub>3</sub> ZnC (alloy 2) plus Calorimeter . . . . .	64
19. Magnetic Specific Heat of Mn <sub>3</sub> AlC . . . . .	66
20. Magnetic Specific Heat of Mn <sub>3</sub> ZnC . . . . .	67
21. Magnetization Curves . . . . .	68b

TABLE INDEX

	<u>Page</u>
I. Measured Capacities of Calorimeter plus Aluminum	
Oxide . . . . .	43
II. Calorimeter Capacity . . . . .	45
III. Capacities of $Mn_3AlC$ plus Calorimeter . . . . .	57
IV. Capacities of $Mn_3ZnC$ plus Calorimeter . . . . .	63

THE CONSTRUCTION OF AN ADIABATIC CALORIMETER  
AND ITS USE IN MEASURING SPECIFIC HEATS.

I. INTRODUCTION

1. Specific Heat Theory

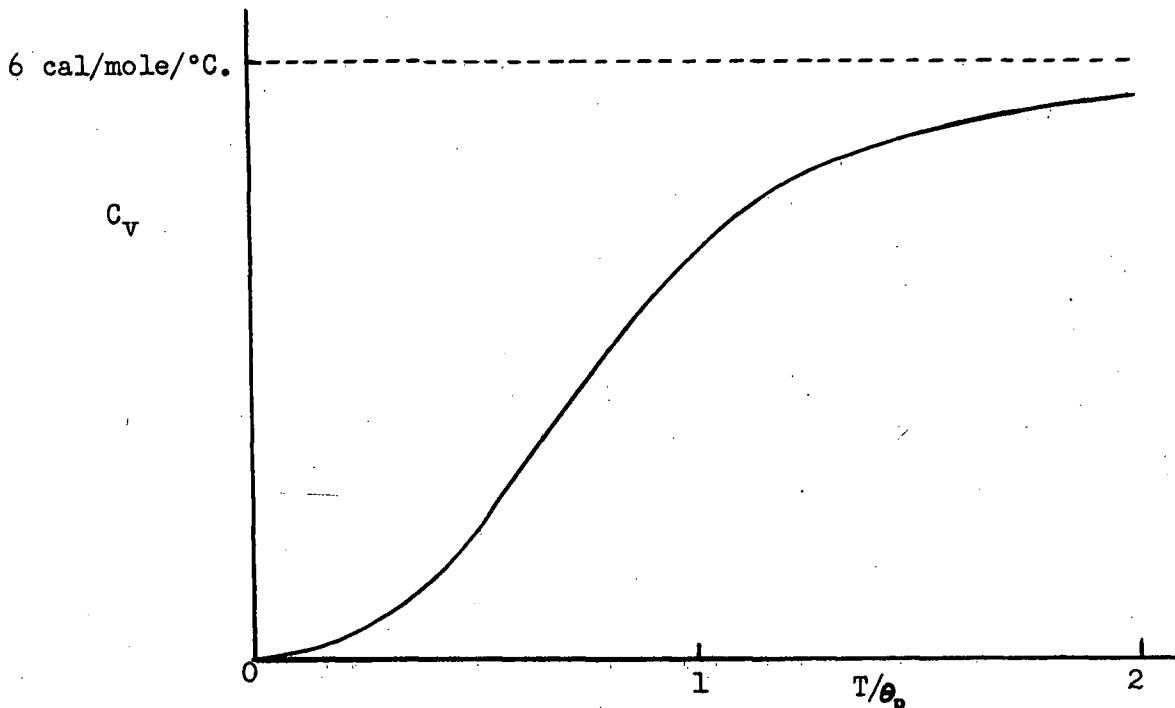
a. General Theory:

The object of the present research is to construct a calorimeter in order to measure the specific heats of certain alloys. From these specific heats, the basic magnetic properties, and consequently the atomic structure of these alloys might be explained.

The specific heat of a substance is defined as

$$C = \delta q/dT$$

where  $\delta q$  is the amount of heat required to change the temperature of a unit mass of the substance by  $dT$ . The specific heat at constant volume for simple substances has been calculated by Debye,<sup>1</sup> the results agreeing well with experiment. If the specific heat of one substance is plotted against  $T/\theta_D$ , where  $\theta_D$  is the Debye temperature, a constant dependent on that substance, the resulting curve is the same as that for many other simple substances.



At high temperatures, the specific heat approaches the classically calculated value of six cal. per mole per degree centigrade, if the electronic specific heat,  $C_e$ , is not considered. However, although the specific heat produced by the electrons is negligible at ordinary temperatures, it becomes appreciable at high temperatures. Moreover, transition metals, which are involved in the present work, often have a larger  $C_e$  than simple metals because of the high density of electron levels in their unfilled 'd' bands.  $C_e$  can be of the order of 6 cal./mole/°C. at very high temperatures for transition metals.

At low temperatures the Debye theory agrees with experimental results, predicting that the specific heat will vary as the cube of the temperature. The present research, however, is concerned with values in the intermediate temperature range ( $0.5 < T/\theta_0 < 1.5$ ), where the slope of the specific heat curve is decreasing rather rapidly.

b. Specific Heat Anomalies:

The present work is devoted primarily to measurement of specific heat anomalies. They are caused by transitions<sup>2</sup> in a substance, which involve a

change of symmetry in the structure of the substance. For a first order transition, the first order derivatives of the Gibbs function,  $G$ , change discontinuously.

$$G = U - TS + PV \quad \text{by definition}$$

where  $U$  = internal energy

$S$  = entropy

$T$  = absolute temperature

$P$  = pressure

$V$  = volume.

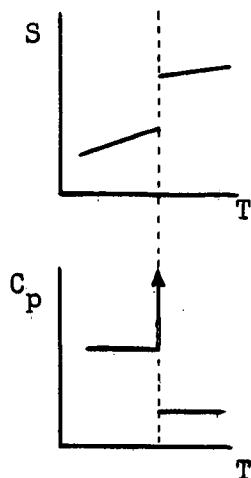
$$dG = VdP - SdT$$

since  $dU = TdS - PdV$

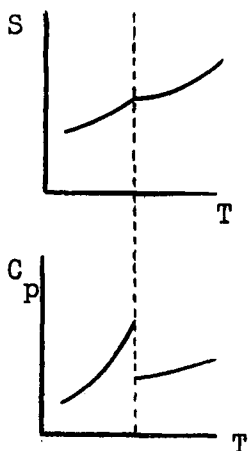
therefore  $\left(\frac{\partial G}{\partial T}\right)_P = -S$

and  $\left(\frac{\partial^2 G}{\partial T^2}\right)_P = -\frac{C_P}{T}$

since  $dS = \frac{C_P dT}{T}$



Consequently, the entropy changes discontinuously for a first order transition (e.g.: melting, vaporization), and the specific heat increases to an infinite value at the transition point (producing a latent heat).



For a second order transition, the first order derivatives of the Gibbs function change continuously and the second order derivatives change discontinuously. Thus a second order transition is accompanied ideally by a discontinuity in the specific heat curve.

Some examples of second order transition are the transitions from an ordered to a disordered state, from a superconductor to an ordinary conductor, and from a magnetic to a non-magnetic state. These transitions all produce similar specific heat anomalies.

The transition pertinent to the present research is the magnetic one. The specific heat anomaly resulting from a ferromagnetic transition can easily be deduced from the theory of Weiss.<sup>1</sup> The energy of magnetization per unit mass of a ferromagnetic substance is

$$U = - \int_0^\sigma H_e d\sigma \quad (1)$$

where  $\sigma$  is the magnetic moment per unit mass, and the effective field

$$H_e = H + NI \quad (2)$$

$H$  is the applied field,  $I$  is the magnetic moment per unit volume and  $N$  is the Weiss intermolecular field constant, which is very large for ferromagnetic materials.

Since  $H$  is negligible in comparison with  $NI$ , and  $I = \rho\sigma$ ,

$$U = - \int_0^\sigma N\rho\sigma d\sigma \quad (3)$$

where  $\rho$  is the density of the substance.

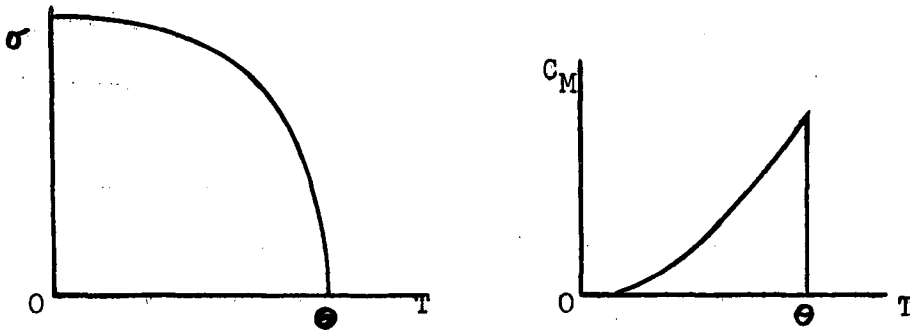
Thus

$$U = - \frac{N\rho\sigma^2}{2} \quad (4)$$

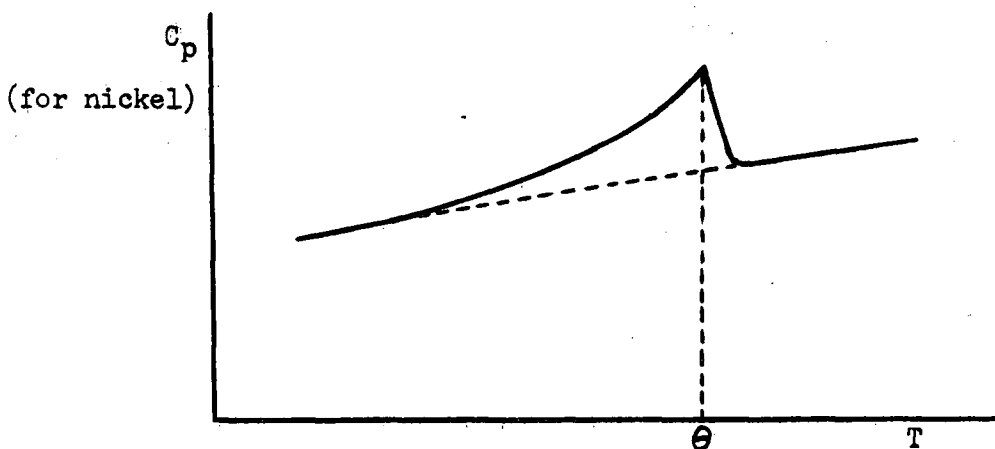
and the anomalous specific heat of magnetization is

$$C_M = - \frac{N\rho}{2} \frac{\partial \sigma^2}{\partial T} = -N\rho\sigma \frac{\partial \sigma}{\partial T} \quad (5)$$

For the theoretical  $(\sigma, T)$  curve,  $C_M$  should rise to a maximum at the Curie temperature,  $\theta$ , and then drop discontinuously to zero.



Since this ideal  $\sigma - T$  curve is never achieved and since perfect experimental conditions can never be attained, the discontinuity has not been observed experimentally. However, it has been approached. The smallest discovered temperature range through which the specific heat drops near the Curie point has been about seven centigrade degrees, observed by Lapp<sup>3</sup> on nickel.



Similar anomalies should occur for antiferromagnetic and ferrimagnetic substances, since large internal exchange forces must exist in them, like in ferromagnetic substances, and the energy of magnetization depends on these

forces between atoms. Whereas in ferromagnetics the spontaneous magnetization vectors of all atoms line up parallel, in antiferromagnetics the vectors of two or more types of atoms oppose, causing zero resultant magnetization. In ferrimagnetics, the vectors also oppose, but do not completely cancel, so that a resultant spontaneous magnetization exists. The anomalies observed for antiferromagnetic and ferrimagnetic substances at their Curie points should be just as large as those observed for ferromagnetic substances if the exchange forces are as large, even though the resultant magnetization may be much smaller.

## 2. The Alloys to be Investigated.

One aim of the present research is to determine the type of magnetization of certain substances by investigating their specific heat anomalies. These substances are single phase alloys of Mn-Al-C and Mn-Zn-C. These alloys have an ordered face-centered cubic 'perovskite' structure and exhibit spontaneous magnetization at room temperature. Because of the great stability of the ordered structure over a wide range of composition, it would seem that bond formation, rather than a normal superlattice attraction, is responsible for the ordering. Of particular interest are the alloys  $Mn_3AlC^4$  and  $Mn_3ZnC^5$ , whose structures have the maximum ordering (see Figure 1).

Mn-Al-C alloys are single phase for a region near the  $Mn_3AlC$  composition. If the carbon content is twenty atomic percent the alloys are single phase for 60-69 atomic percent Mn and thus for 20-11 atomic percent Al. The lattice parameter is 3.869 Å for  $Mn_3AlC$  and varies little with composition, indicating that the Mn and Al atoms have almost the same diameter. In these alloys the saturation magnetization below the Curie temperature varies with temperature in a normal ferromagnetic manner, but the paramagnetic behaviour above the Curie point indicates ferrimagnetism, or at least a departure from Curie-Weiss behaviour. Neutron

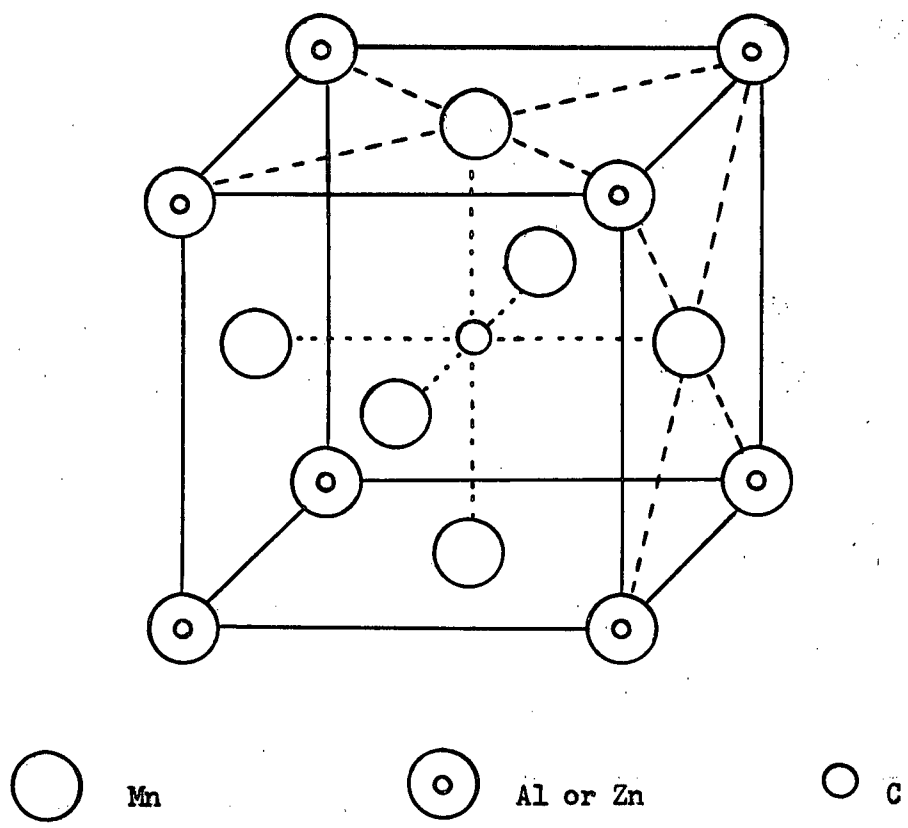


Figure 1: Perovskite Structure.

diffraction results indicate that  $Mn_3AlC$  is ferromagnetic above liquid helium temperature.

As the Mn content is increased from 60 to 69 atomic percent, the Curie temperature increases from  $0^\circ C$  to  $300^\circ C$ , while the saturation magnetization decreases from 1.20 to 0.6 Bohr magnetons per Mn atom. This decrease in magnetization as the Mn content is increased past the value for maximum ordering (60 atomic percent Mn) can be explained in one way by assuming that the magnetization of the additional Mn atoms (which must replace Al atoms in cube corner positions) is antiparallel to that of those in face-centered positions. The magnitude of the decrease in magnetization corresponds to the extra Mn atoms having an approximate effective Bohr magneton value of  $\mu = -4\mu_B$  (see Appendix I). (This, incidentally, is the value of  $\mu$  for manganese in the Heusler alloys).

This interpretation could possibly be verified by specific heat measurements. By simple Weiss theory, the height of the specific heat anomaly varies directly as the Bohr magneton number for a ferromagnetic substance. Thus, if the Mn-Al-C alloys were always ferromagnetic, the height of the anomaly and also its total size would become smaller as the magnetization decreased. But for a ferrimagnetic alloy, the anomaly's height depends on the Bohr magneton number of the separate atoms. Thus, the anomaly height would increase while the magnetization decreased if the extra manganese atoms had large negative  $\mu$ , as hypothesized. Moreover, other things being equal, the total size of the anomaly would increase if Mn atoms of large negative  $\mu$  were added to the alloy (see Appendix II).

The Mn-Zn-C alloys, like the Mn-Al-C alloys, are single phase over the range of composition from  $Mn_{60}Zn_{20}C_{20}$  to  $Mn_{70}Zn_{10}C_{20}$ . The lattice parameter of  $Mn_3ZnC$  is  $3.925\text{\AA}$  and it varies only slightly with composition. The Curie

temperature varies from about 80°C for Mn<sub>3</sub>ZnC to ~500°C for Mn<sub>70</sub>Zn<sub>10</sub>C<sub>20</sub>. The variation of the saturation magnetization for the alloys with Mn content near 60 atomic percent is unusual at low temperatures.<sup>5</sup> (see Figure 2). The magnetization has a maximum near -40°C, corresponding to the behaviour at low temperatures predicted by Néel (see Appendix II) for one type of ferrimagnetic substance. The paramagnetic behaviour above the Curie point also appears to agree with that predicted by Néel for ferrimagnetics. He deduced that the inverse of the susceptibility,

$$\frac{1}{\chi} = \frac{T}{C} + \frac{1}{\chi_0} - \frac{\sigma}{T - \theta} \quad (\text{see Appendix II})$$

The curvature of the resulting ( $\frac{1}{\chi}$ , T) curve is concave to the temperature axis, rather than convex, as is usual for a ferromagnetic substance.

However, neutron diffraction experiments carried out at Chalk River by Dr. B. Brockhouse<sup>6</sup> on the alloy of approximate composition Mn<sub>3</sub>ZnC suggest a different and entirely new magnetic concept to explain the magnetic properties of this alloy. These experiments indicate that between the transition temperature of -40°C and the Curie temperature, Mn<sub>3</sub>ZnC is a normal ferromagnetic substance with magnetically equivalent manganese atoms. But below the transition temperature, a complex magnetic structure exists. The actual structure is unknown, but one in good agreement with neutron diffraction and magnetic data is that proposed by B.N. Brockhouse and H.P. Myers.<sup>6</sup> Manganese atoms having magnetic moments of zero, two and three Bohr magnetons are arranged as shown in Figure 3 for the state at absolute zero temperature. The magnetic moments of the 2 $\mu_B$  manganese atoms are opposing, so that the algebraic mean moment of the alloy is 1 $\mu_B$  per manganese atom at 0°K, in agreement with magnetic measurements. If the magnetic moments of the manganese atoms above the transition temperature were the same as their arithmetic mean moment in the low temperature structure, then the ferromagnetic moment extrapolated to 0°K would be 1.66 $\mu_B$ . This is in good

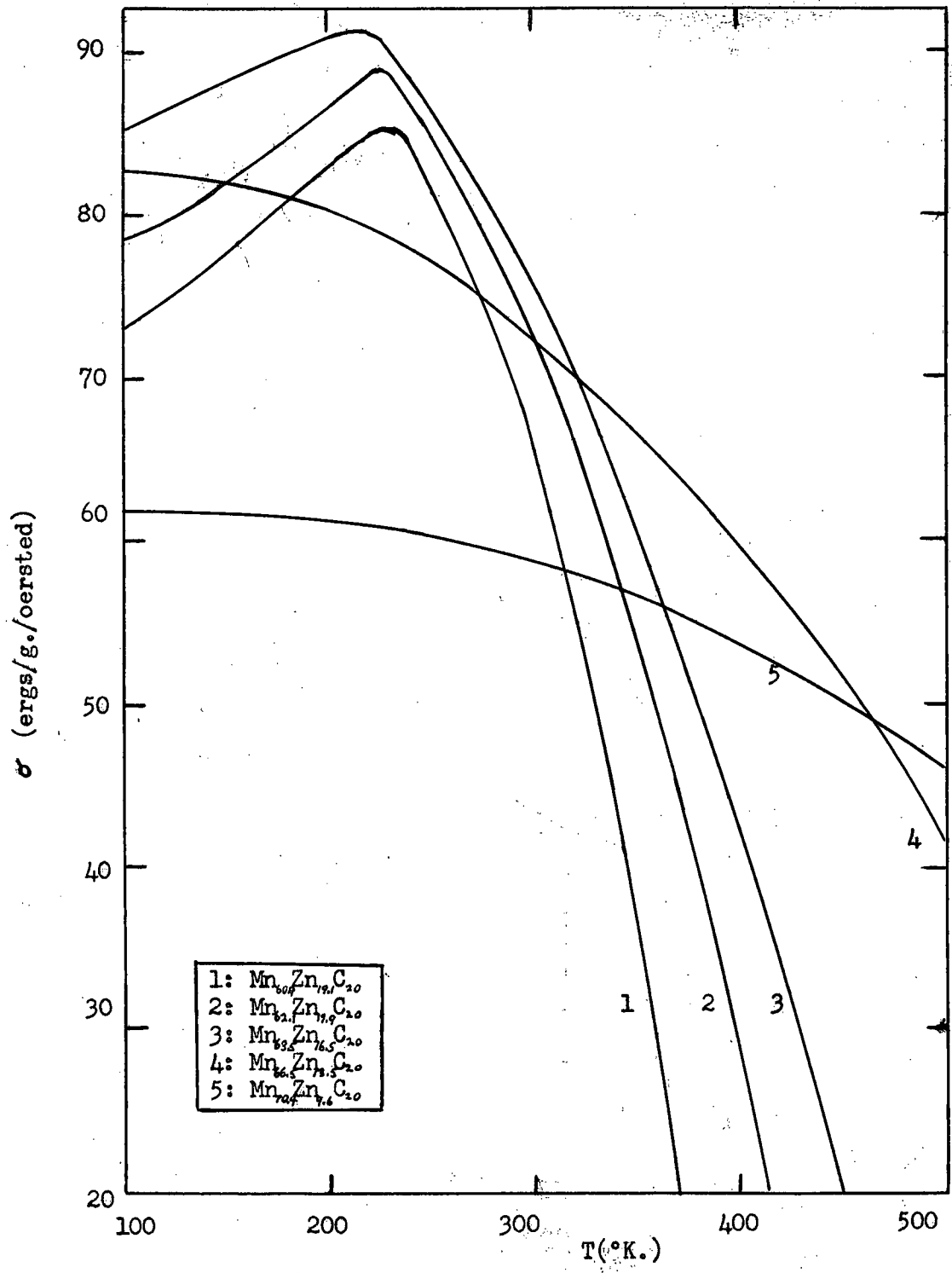


Figure 2: Variation of Saturation Magnetization,  $\sigma$ , with Temperature, T, for Mn-Zn-C Alloys

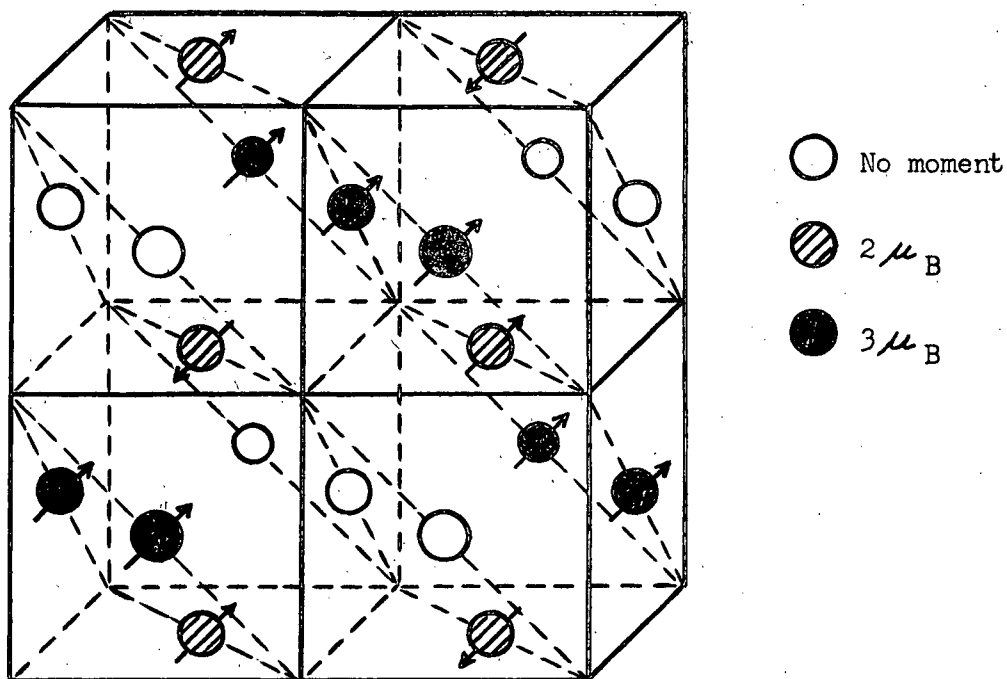


Figure 3. Possible Magnetic Structure  
at 0°K of Mn<sub>3</sub>ZnC.

Only one half of the large unit cell is shown; the other half is similar but displaced one-half unit along the  $x$ -axis. Only manganese atoms are shown. The moments are oriented along a  $[111]$  diagonal.

agreement with the experimental extrapolated value of  $1.5\mu_B$ .

At the transition temperature the magnetic moments of the proposed complex lattice must rearrange themselves to become equivalent. This rearrangement involves a change in interatomic exchange forces, so that a second order specific heat anomaly comparable to that occurring at the Curie temperature should be observable. In order to understand the form of the experimental magnetization curve for  $Mn_3ZnC$  in terms of the two magnetic structures mentioned, one may consider that below the transition point an opposing sublattice of magnetic moments comes into effect. The Curie temperature of this fictitious lattice is the transition temperature.

Although the cubic structure of  $Mn_3ZnC$  becomes slightly distorted into a face-centered tetragonal structure ( $c/a = 0.995$ ) near  $-40^\circ C$ , this phase change is gradual, so that no appreciable first or second order anomaly should result. Thus, if the ferrimagnetic model for  $Mn_3ZnC$  were correct, the only anomaly which would occur at  $-40^\circ C$  would be a small third order one.

It is seen that measurement of specific heat anomalies should prove very useful in checking the validity of magnetic models and thus in determining basic atomic structures of alloys.

### 3. Calorimetric Theory<sup>7</sup>

#### a. General Theory:

The specific heat of a substance is measured by means of a calorimeter, which is a device into which heat can be introduced and the resulting temperature change measured. Part of the heat brought into the calorimeter raises its

temperature and part is lost to the surroundings. In precise calorimetric measurements, the temperature change of the calorimeter and its thermal leakage (the amount of heat lost from the calorimeter during the measurement) must be accurately determined. Since the greatest calorimetric error frequently arises from measurement of the temperature change, an accurate thermometer must be used. For precise work, a platinum resistance thermometer<sup>8, 9</sup> is most often used. The resistance of pure platinum, varying almost linearly with temperature, follows a smooth curve which is determined by calibration at International Temperature Scale fixed points. Because of its stability, strain-free platinum does not require recalibration very often. A platinum resistance thermometer, used with a Mueller bridge, will measure temperatures to 0.001°C accuracy in the intermediate range.

For less accurate work, thermocouples may be used; they have the advantage of having practically no heat capacity, but are inaccurate because of thermal gradients. Mercury thermometers, besides having little accuracy, can be used for only very restricted temperature ranges, and are not suitable for vacuum apparatus.

Most of the types of calorimeter design are the result of thermal leakage considerations. The leakage depends on the thermal head,  $\phi$ , which is the temperature difference between the calorimeter and its surroundings. The formula usually used to calculate the leakage is  $\eta = \phi kt$ .  $\eta$  is the temperature change in the calorimeter caused by the leakage for an experimental time  $t$ .  $k$  is the thermal leakage modulus of the calorimeter.

In the ordinary calorimetric method, since the thermal leakage is relatively high, it must be accurately estimated. To do this,  $k$  is found by measuring  $\eta/t$  and  $\phi$  for a rating period immediately after each experimental period, and it is assumed to be the same in the experimental period. In order to

measure the thermal head,  $\phi$ , accurately, the calorimeter vessel surroundings must be at a constant uniform temperature; a water jacket is often used for this purpose. The temperature change of the rating period must also be accurately measured. Because the error in measuring this temperature change must be added to the temperature error of the experimental period, the total thermometric error is doubled by the leakage correction.

Since the thermal leakage modulus varies with temperature and other conditions, it must be measured after each experimental period for accurate results, unless its variation is greatly reduced by some experimental arrangement. The vacuum-jacketed calorimeter invented by Dewar decreases the thermal leakage modulus, so that  $\phi$  need not be so precise in order to accurately estimate  $\eta$ . In Joule's method, twin calorimeters are heated the same amount, so that the thermal leakage, temperature, and heat capacity determinations become comparative measurements, made with differential apparatus. Other methods, such as the adiabatic method, indirectly reduce the errors involved in estimating the thermal leakage.

b. The Adiabatic Calorimeter

In the adiabatic calorimeter, the thermal head is reduced almost to zero by keeping the temperature of a jacket or shield almost equal to that of the calorimeter vessel. Thus, since the thermal leakage is greatly reduced, it is usually neglected. But because the error involved in adjusting the jacket temperature for adiabatic conditions is greater than that in measuring the thermal head, the resulting error in the thermal head is greater for the adiabatic method than for the ordinary method. And so the leakage neglected in the adiabatic method may be greater than the error in the leakage calculation for the ordinary method.

One advantage of the adiabatic method is that it reduces the effect of variations in the leakage modulus, which are a chief source of error in non-

adiabatic methods. The smallness of the thermal head reduces the effect of fluctuations in the leakage modulus in two ways: First, the fluctuations during an experiment are caused mostly by convection, which is directly dependent on the thermal head. Second, any change in the leakage modulus will cause a corresponding change in the thermal leakage; but the thermal leakage is already negligible, so that any such change in it will also be negligible.

Because leakage modulus variations are reduced by the adiabatic method, it is especially useful for protracted experiments, for which the leakage modulus might ordinarily change considerably. Also, although large temperature rises can not be used with accuracy for non-adiabatic methods, because of the convection effects, they can be successfully used with the adiabatic method. Consequently, the important temperature measurement errors can be greatly reduced. A temperature rise increase from two to ten degrees, for example, would reduce the temperature measurement error by four fifths. Moreover, larger temperature rises will permit more rapid measurement of a specific heat curve. The adiabatic method avoids the ordinary rating period, in which the leakage modulus is found, but a period is often required for which any constant temperature drift (such as caused by the heat of stirring) is determined.

The aneroid, or fluidless, adiabatic calorimeter, by eliminating stirring, may almost completely eliminate temperature drift. Thus no corrections for leakage need be made, and considerable time and calculations are avoided. One experimental period can follow another without pause for large temperature ranges. Extreme temperatures can be much more easily attained with an aneroid calorimeter than with one containing fluids.

Another advantage of the aneroid method is that small dimensions (and less dead material) are possible for the calorimeter, because of the absence of

fluid circulation problems. Smaller dimensions mean faster thermal equilibrium and thus a shorter experimental time (producing less total thermal leakage), which is usually an advantage. However, at very low temperature, since the main heat loss is by conduction along wires, smaller dimensions are not so advantageous.

The main disadvantage of the aneroid calorimeter is that the temperature equalization must be by conduction alone. In order to speed the conduction:

- (1) Metal of high conductivity (copper or silver) is used.
- (2) The heat is generated uniformly.
- (3) The thermal head is kept small, so that temperature differences are not produced by thermal leakage. The adiabatic method is thus especially useful.

Necessary to the aneroid adiabatic calorimeter is the measurement of the thermal head between calorimeter and shield. The most convenient way to do this is with thermocouples. The lag of the thermocouples should present no problem, since it is small and probably constant. If only a few couples are used, the average of the thermal heads measured may not be the correct average head, unless the thermal equilibrium is very good for both calorimeter and shield. Thus, pains should be taken to insure good thermal equilibrium.

The aneroid adiabatic calorimeter was chosen as most suitable for the present work, because of the following reasons:

- (1) It can give suitable accuracy (approaching 0.2%) for the temperature range required: -150 to 150°C.
- (2) It can give quick and simple measurements, especially if the rating period is eliminated.

- (3) It can be constructed simply and economically, even though the adiabatic controls introduce some complexity.

## II. THE CONSTRUCTION OF AN ANEROID ADIABATIC CALORIMETER

### 1. Design

#### a. General Aim:

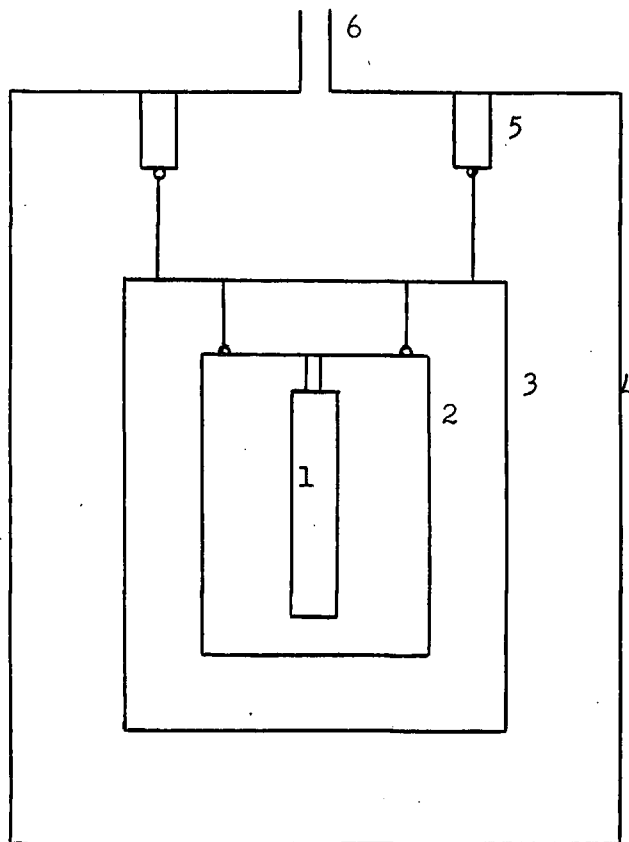
The basic design required was one of simplicity coupled with accuracy, since the simplest construction which will still give the required accuracy is undoubtedly the most desirable. The precision desired for the calorimeter was approximately 0.5%, with a reduction to 0.2% possible by means of modification.

Fast operation of the calorimeter by one person was desirable, for convenience as well as economy. The calorimeter must be operable for samples in powder form over the temperature range  $-150$  to  $150^{\circ}\text{C}$ , since the alloys to be measured required this. Also, adaptability to samples of a different form was advantageous, with regard to future use of the calorimeter.

#### b. Basic Design:

The basic design<sup>10</sup> of the adiabatic calorimeter is shown in Figure 4. The cylindrical calorimeter vessel (2) contains the specimen whose specific heat is to be measured, and the platinum resistance thermometer-heater (1). The vessel is filled with helium for good conduction. The thermometer-heater is used, in conjunction with standard resistances and a potentiometer, to measure accurately the heat it has introduced to the vessel and the resulting temperature change.

The adiabatic shield (3) is heated electrically so that its temperature remains close to that of the vessel, and thermal leakage may be neglected. The temperature difference between vessel and shield is measured with thermocouples



- 1: Thermometer-Heater
- 2: Calorimeter Vessel
- 3: Adiabatic Shield
- 4: Outer Case
- 5: Brass Ring
- 6: Evacuation Tube

Figure 4: Basic Calorimeter Design

connected to a galvanometer. The outer case (4) is evacuated through the tube (6) so that thermal leakage between the shield and the vessel, and between the shield and the case is reduced. In order to reduce thermal leakage through the leads, they are wrapped around the shield and the brass ring (5) before emerging through the evacuation tube.

## 2. Materials and Detailed Construction<sup>11, 12</sup>

### a. The Calorimeter Vessel:

#### (i) Theory:

To promote fast conduction, the calorimeter vessel was made of copper. By placing the thermometer-heater in the center of the vessel, the heat was generated uniformly, and thermal equilibrium was speeded. Also, a central position of the heater made more gradual the temperature change of the vessel surface, so that the adiabatic control was easier.

The calorimeter vessel was made an air-tight cylindrical container, so that it could accommodate practically any type of solid material, and in particular the powdered, easily corroded substances which were to be investigated.

The size of the calorimeter vessel depends on several factors. As mentioned earlier, smaller dimensions result in faster thermal equilibrium, which is advantageous. However, the leakage modulus will increase as the dimensions decrease, since it varies directly as the surface area but inversely as the heat capacity or volume; if the dimensions decrease by 'n' times, the leakage modulus is  $n^3/n^2 = n$  times as large. However, for a smaller calorimeter, the shortening of the experimental time caused by faster equilibrium may more than compensate for the increased leakage modulus, and produce less total thermal leakage.

For very small dimensions, technical difficulties are encountered. Also, the increase in weight of the calorimeter vessel with respect to the

weight of the sample decreases the precision. Thus for the calorimeter constructed here, a compromise size was chosen, which enabled the sample weight to be larger than the vessel weight, while still retaining quite rapid equilibrium conditions.

(ii) Construction: (see Figure 5)

The calorimeter vessel (2) is a silver-plated cylindrical copper container, approximately 4 by 5 cm. (1.57 x 1.97 in.), and 0.05 cm. thick (.020 in.). It was made by electroplating copper onto a stainless steel mold having a 1/4° pitch and shouldered to facilitate removal. The electrolysis solution was a dilute sulphuric acid solution of  $\text{CuSO}_4$  containing a small amount of gelatin. A plating current of 0.3 amperes for 120 hours was used, corresponding to a thickness of 0.044 in., and the excess copper was machined off to the required thickness.

The calorimeter vessel was silver-plated inside and out (to reduce the radiation of heat) to a thickness of  $\sim 0.003$  in. The solution used contained:

AgCN	36 g./liter
KCN	52 g./liter
$\text{K}_2\text{CO}_3$	38 g./liter

A small amount of  $\text{CS}_2$  was added as a brightener. A current of 1 ampere (current density of 5 amp/sq.ft.) and a voltage of 1 to 2 were used.

The bottom of the calorimeter vessel was soft soldered on. The thermometer (1) was fixed within the vessel and its leads (3) exited from the vessel by soft soldering a disk connected to the thermometer onto the top of the vessel. (The thermometers used will be described in detail later).

A kovar metal-glass seal (4) (No. 96.1010 from the Stupakoff Ceramic and Manufacturing Co.), soldered through the top of the vessel, was used to admit

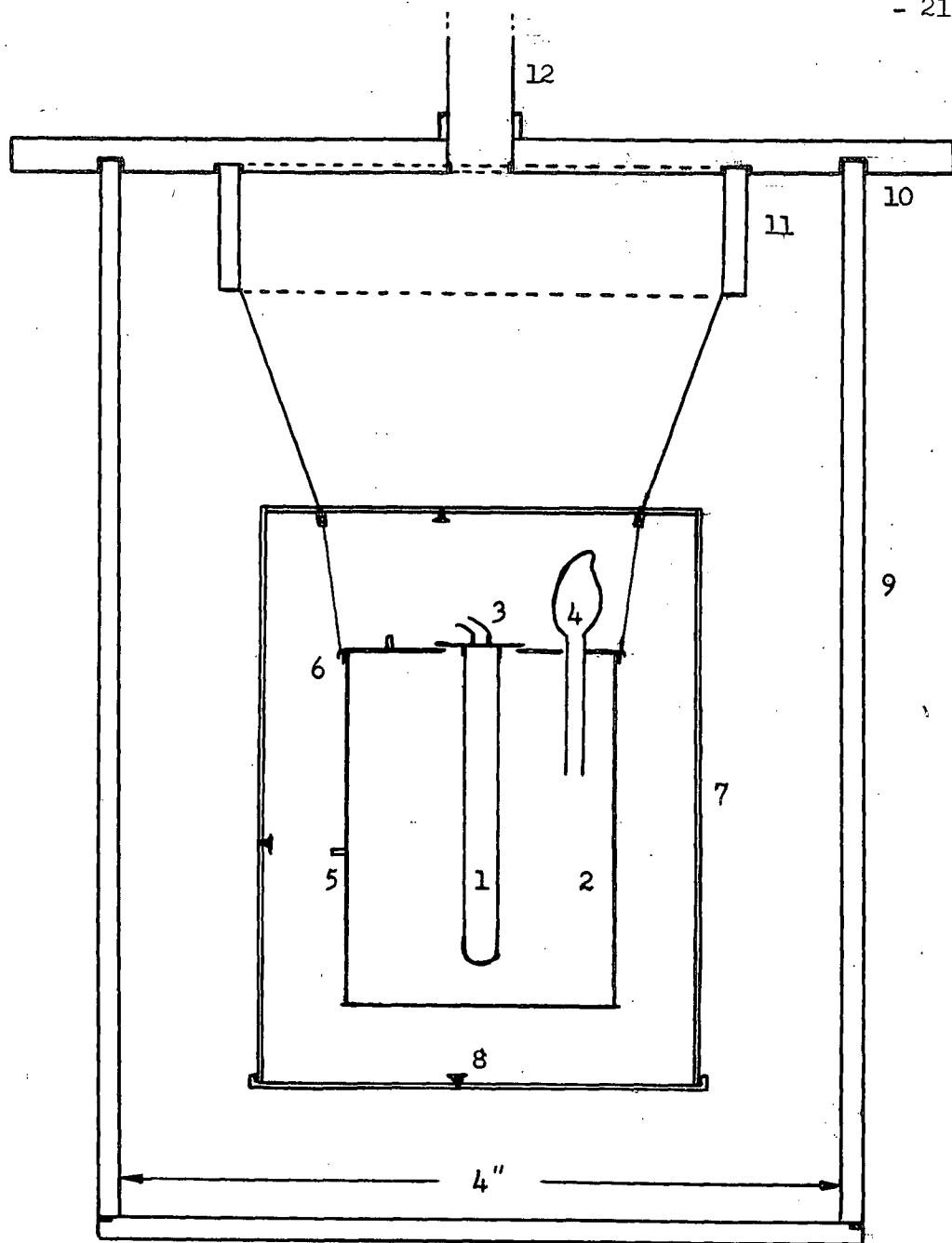


Figure 5: The Calorimeter (Actual Size)

helium to about four fifths atmospheric pressure, in order to speed thermal equilibrium. After the helium was introduced to the vessel, the glass tube of the seal was drawn off in an oxygen-gas flame. In order to change samples to be measured in the vessel, the kovar seal and thermometer were removed, and the sample was admitted through the vessel top. The total weight of the calorimeter vessel plus thermometer was about 43 g.

Binding posts (5) were soldered to the side and top of the calorimeter vessel for thermocouple connections. Three wire hooks (6) were soldered to the vessel top for suspension of the calorimeter within the shield.

b. The Adiabatic Shield

(i) Theory:

The adiabatic shield must be heated so that its temperature remains close to that of the calorimeter vessel surface. In order to keep the shield surface temperature uniform, the shield must be a highly conducting material. The uniformity of surface temperature is especially desirable if only a few thermocouples are used to determine the temperature. To lessen temperature lags, the heat capacity of the shield must be small, and thus the shield walls must be thin. The shield must not be air-tight, since a vacuum between shield and calorimeter vessel is necessary to reduce thermal leakage.

(ii) Construction: (see Figure 5)

The shield (7) is a 6 by 8 cm. (2.4 x 3.2 in.) cylindrical brass container, 0.07 cm. (.030 in.) thick, with a removable bottom. It was made by reducing brass tubing to the desired thickness in an acid bath, and silver soldering on a brass top. The bottom was machined into a friction-fitting cap.

The shield was heated by means of a non-inductive uniform winding of

No. 32 gauge silk-covered manganin wire. The total resistance of the winding was 420 ohms: 300 ohms for the side and 60 ohms each for the top and bottom. The wire was insulated and connected to the shield with Dow Corning 935 varnish. This is a silicone electrical insulating varnish having good flexibility from  $-55^{\circ}$  to  $260^{\circ}\text{C}$ . It dries tack-free in three hours at  $200^{\circ}\text{C}$ . The winding onto the shield was accomplished in stages, the varnish being baked after each few windings.

In order to prevent conduction along the thermocouple and thermometer leads (No. 29 B. and S. Cu formex), they were wrapped non-inductively around the outside of the shield under the manganin winding. Aluminum foil was cemented onto the shield surfaces (with the same varnish) in order to reduce radiation of heat.

Three small screws (8) were fastened to the shield side, top and bottom for thermocouple connections. Differential copper-constantan thermocouples (No. 30 B and S, insulated with the varnish) were attached from the shield side to the shield top, the shield bottom, the calorimeter vessel side, and the calorimeter vessel top. Thus all temperatures were found relative to the shield side temperature. Three small holes through the shield top permitted suspension with threads of the calorimeter vessel within the shield and the shield within the outer case.

### c. The Adiabatic Shield Controls

The differential copper-constantan thermocouples were used to find the temperature difference between the shield side and shield top, shield bottom, calorimeter side and calorimeter top. The thermocouples were connected to a Leeds and Northrup galvanometer having a sensitivity of  $0.6 \mu\text{V}$  per mm., giving a deflection of 60 mm per  $^{\circ}\text{C}$  at room temperature. Any one of the four differential thermocouples was connected to the galvanometer at one time. (see Figure 6b).

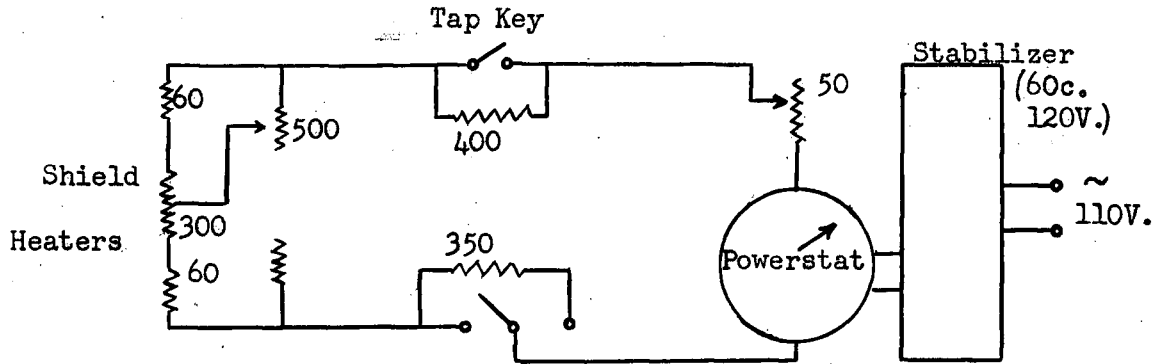


Figure 6a: Power Control

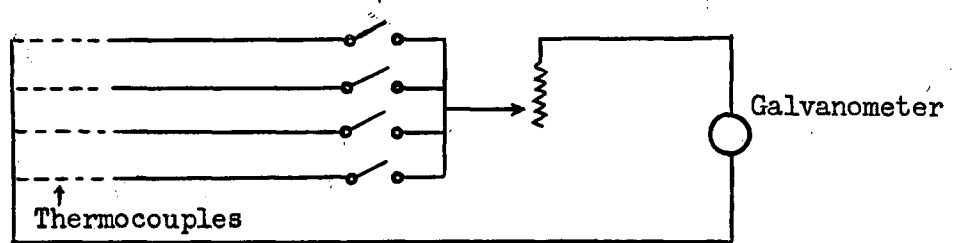


Figure 6b: Thermal Head Measurement

Figure 6: Adiabatic Shield Control Circuit

The manually operated power control circuit for the adiabatic shield is shown in Figure 6a. The power was supplied by a 60 cycle 120 volt stabilizer. A 0-110 V powerstat permitted power control; the fine control, obtained with a 50 ohm variable resistance, was not normally used. The current was raised briefly by means of a tapping key shunting out a 400 ohm resistance, and the current was lowered briefly by switching a 350 ohm resistance into the circuit. Part of the current was shunted from the top shield heater through a variable 500 ohm resistance in order to equalize the shield top and bottom temperatures.

Since the controls became difficult for a temperature difference of more than 50°C between the shield and outer case, the difference was kept smaller by controlling the case temperature.

d. The Outer Case

(i) Theory:

The outer case serves primarily as an evacuation chamber to make temperature control easier. When it is evacuated, the thermal leakage between the adiabatic shield and the calorimeter vessel is decreased greatly, enabling the leakage to be neglected. Equally important, the leakage between the shield and the outer case is reduced, so that the shield temperature control is simplified.

By keeping the outer case temperature near the shield temperature, the shield control is made still easier. The case temperature was controlled by immersing in a temperature bath in a Dewar flask. For temperatures up to 90°C, a water bath was used, containing a heating element supplied with a variable alternating voltage. For low temperatures, down to -80°C, a mixture of dry ice and acetone was used. For temperatures from -80°C to -160°C, liquid oxygen was fed through a copper coil immersed in gasoline; the gasoline was first cooled to -80°C with dry ice.

(ii) Construction: (see Figure 5).

The outer case (9) is a 10 by 15 cm. (4 x 6 in.) copper cylinder, 0.2 cm. thick (1/8 in.), with a brass bottom soft soldered on, and a removable brass cover. A groove was machined into the cover, so that it could fit onto the case in a vacuum grease seal (10) (Dow Corning high vacuum grease was used). To reduce thermal conduction along the leads, they were wrapped around a brass ring (11) (1/8" thick and 3/4" long) soldered onto the inside of the cover. Three holes were drilled through the ring for suspension of the shield.

The case was evacuated through a thin walled 3/8" German silver tube (12), silver soldered to the cover. A glass T-tube was connected to the German silver tube, so that the leads might emerge from the vacuum system through one arm of the T-tube, which was sealed with de Khotinsky wax. Flexible leads were soldered to the No. 29B and S Cu formex leads where they emerged from the system, and the junctions were fixed with de Khotinsky wax.

The case was suspended within the Dewar flask on a plate held by three 1/8" threaded steel rods, as shown in Figure 7.

e. The Thermometer-Heater

(i) Theory:

A platinum resistance thermometer-heater<sup>8, 9</sup> was used both to supply heat to the calorimeter vessel and to measure the vessel temperature. This dual purpose can be accomplished for an adiabatic calorimeter, since no temperature measurement need be made while energy is being supplied to the calorimeter vessel. The double use of the thermometer enables all temperature and heat input measurements to be made with one potentiometer. The disadvantage of a thermometer-heater is that the error in heat input measurement is increased, unless special precautions are taken, because of the variation of resistance of the heater with temperature.

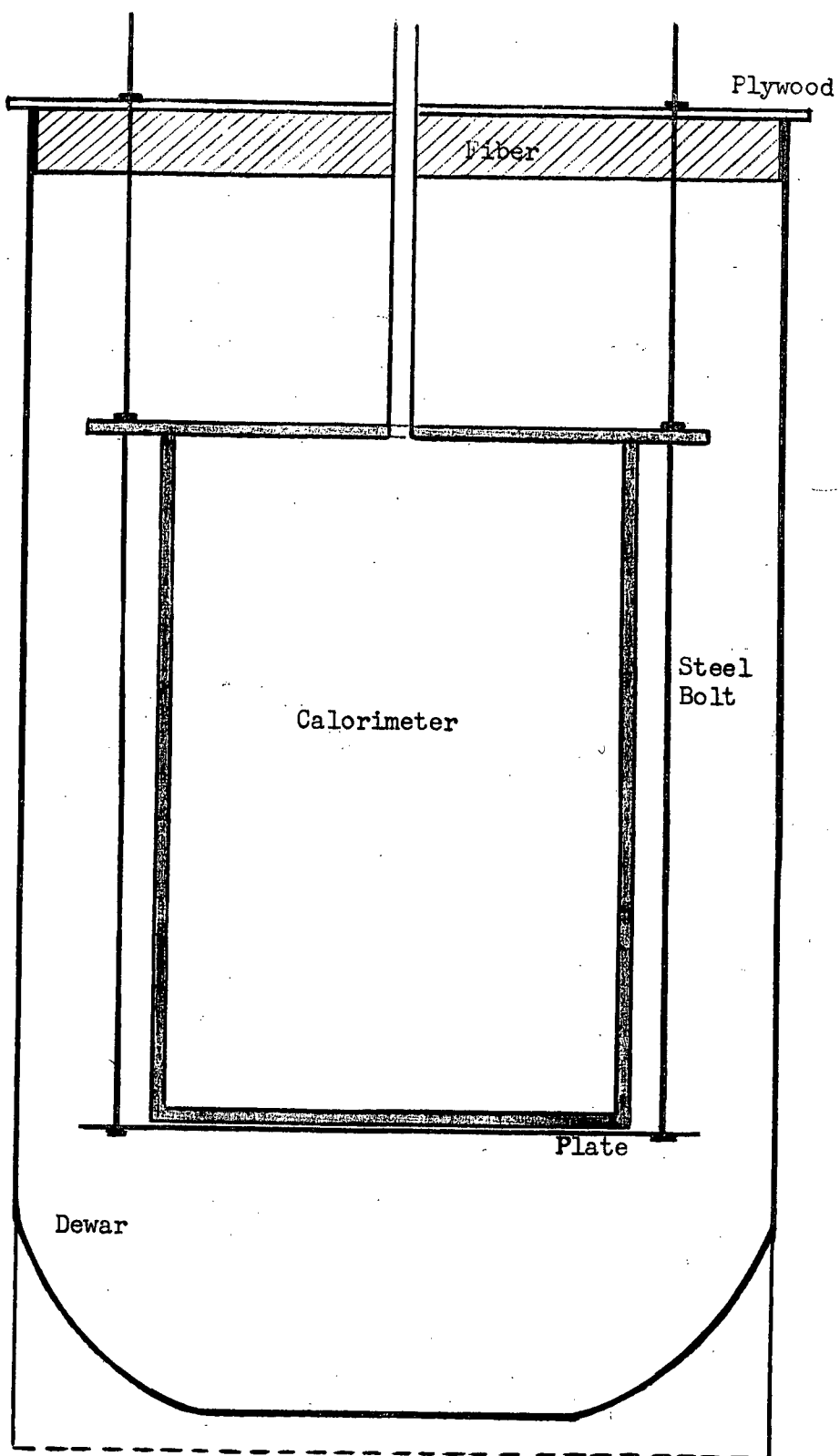


Figure 7: Suspension of the Calorimeter

(ii) Construction: Two different kinds of platinum resistance thermometers were used.

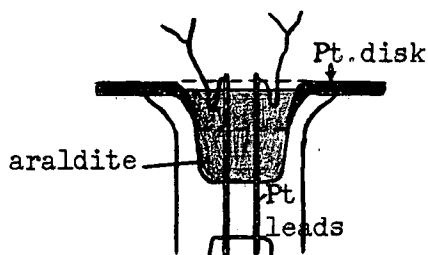
(a) Glass embedded coil: A commercial 100 ohm platinum resistance thermometer (produced by Wheelco Co., now Barber-Colman Co.) was used first. It consists of a non-inductive winding of fine platinum ribbon embedded in a soft



Thermometer;  
Actual Size

glass tube (0.17 in. x 1.75 in.). The two 0.010 in. platinum leads emerge from a cup-shaped top.

A platinum disk, 0.005 inches thick and 0.5 inches diameter, punched so that it fitted into the cup, was sealed to the glass by heating it by induction to a bright red color. Flexible copper leads were soft soldered to the platinum leads, doubled back into the cup, and fixed there with araldite cement. Two leads were soldered to each flexible lead to make the four-lead type of thermometer. (The resistance of the two flexible leads - 0.01 ohm - was negligible in comparison with the platinum resistance).



The thermometer was fixed within the calorimeter vessel by soft soldering the platinum disk to the vessel top.

The disadvantage of this type of thermometer is that its calibration varies because of strains produced in the platinum by expansion of the glass.

(b) Strain-free thermometer: In order to avoid repeated thermometer calibration, a strain-free platinum resistance thermometer was constructed. The thermometer must be small, in order to fit into the calorimeter and to have fast

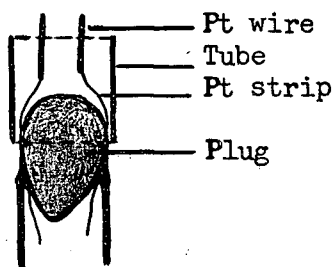
thermal equilibrium, but the platinum wire must be free to expand and have no possibility of short circuits. The usual method<sup>13, 14</sup> of satisfying these conditions is to wind fine platinum wire into a small diameter coil and then wind the coil around an insulating support (usually mica). The whole is then enclosed in an air-tight container, to avoid contamination of the platinum and water condensation on it, as well as for mechanical protection.

This was the method adopted. Chemically pure platinum wire 0.003 in. diameter was used. The specifications ensuring purity are that the ratio of the resistance at 100°C to that at 0°C is greater than 1.390 and the ratio of the resistance at -183°C to that at 0°C is less than 0.250. From 100 to 200 cm of the wire was wound under 10 g tension on a stretched steel wire mandrel 0.010 in. diameter. The helix, from 2.5 to 5 inches long, was slipped off the mandrel and stretched to about 10 inches, so that none of the coils were in contact. The platinum helix was then wound under 1 g tension non-inductively around a notched mica cross held in a mandrel. For assembly of the mica cross see Appendix III.

One 20 ohm and one 50 ohm thermometer were constructed.

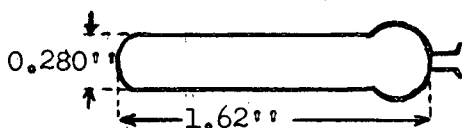


Of the many types of protective case materials used for resistance thermometers, pyrex glass was chosen because it is easy to work and is suitable for the temperature range desired. Thin-walled pyrex was used for the protective tube, and thin platinum strips were used for leads in order to make a vacuum seal through the glass. The sealing procedure is detailed in Appendix IV.



The platinum strips emerging from the seal were fused to 0.020 inch platinum wire leads. The wire was flattened at one end by rolling, was held in contact with the platinum strip by pincers, and was fused with an oxy-gas flame. A pyrex tube was then fitted over the leads and collapsed, so as to fix the platinum strips and leave only the heavy platinum leads emerging from the thermometer.

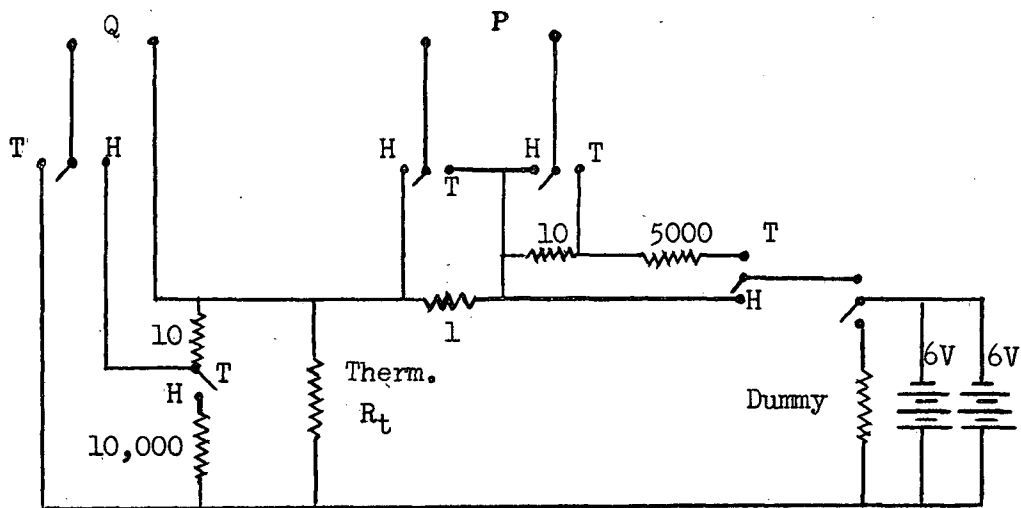
The thermometer was then cleaned in a dilute nitric acid solution, annealed for 15 hours at 490°C, and de-gassed for 3 hours at 400°C. After the seal was leak-tested, the thermometer was filled with dried helium at two-thirds atmospheric pressure and the pyrex tube was sealed off. The actual size of the thermometer is shown in the diagram.



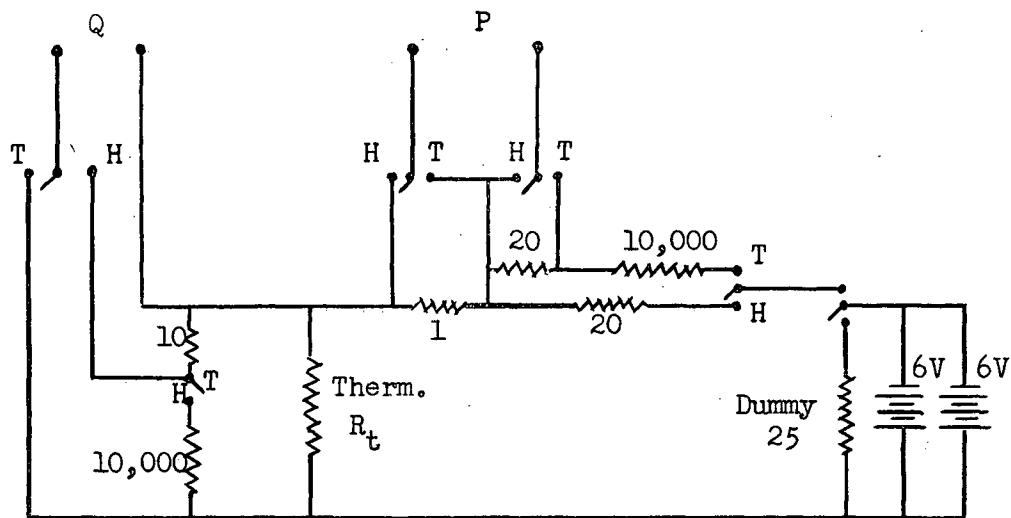
Kovar seals were used to attach the thermometer to the calorimeter vessel and to bring its leads out of the vessel. The two platinum leads were soldered to kovar seals, which were soldered to a silvered phosphor bronze disk. This disk was soldered to the calorimeter vessel top. Two fine leads were connected to each kovar seal on the outside. The resistance of the kovar seals ( $\sim 0.001$  ohm) is negligible in comparison with that of the resistance thermometer.

f. Energy Input and Temperature Measurement

The potentiometer method was used to measure both the thermometer resistance, for temperature determinations, and the energy input to the thermometer when used as a heater. Both measurements were made with one potentiometer, using one circuit. The circuit, which was slightly different for the commercial 100 ohm thermometer and the strain-free 20 ohm thermometer, is shown in Figure 8.



a. Commercial 100 ohm Thermometer Circuit



b. Strain-free 20 ohm Thermometer Circuit.

Figure 8. Circuit Diagrams for Thermometer-Heaters.

To produce a very stable direct current source, six 120 amp.-hour 2 volt storage batteries were used. They were arranged to create two 6 volt sources in parallel. Before an energy input, the batteries were discharged through a dummy resistance, so that their voltage would be constant while measurements were being made. For temperature measurements, the switches were thrown to position T in Figure 8, and for heat input the switches were at position H.

The potentiometer connections are at P and Q. A Tinsley type 3387B potentiometer was used, having ranges 0 to  $1.9 \times 10^{-2}$ ,  $1.9 \times 10^{-1}$  and 1.9 volts, readable to 0.005% or  $\frac{1}{19,000}$  of the maximum. The accuracy is 0.01% of the maximum, or  $2 \mu$  V for the lowest scale. All resistances, the potential across which was to be measured, were standard resistances. All leads inside the calorimeter were No. 29B and S copper, formex insulated, and outside were No. 18B and S flexible copper.

(i) Energy Input:

The potential across the heater was found by using a potential divider, consisting of a 10 and a 10,000 ohm resistance. The potential across the 10 ohm resistance was measured; it was

$$V_Q = \frac{10}{10,010 + R_{\text{leads}}} \text{ times}$$

the potential across the heater. Since the resistance of the leads was about 1 ohm, the potential across the heater,

$$V = 1001.1 V_Q ;$$

neglecting the lead resistance produced an insignificant error of 0.01%.

The current through the heater was found by measuring the potential across a 1 ohm standard resistance. This potential,  $V_p$ , was equivalent to the

total current through the circuit. The current through the heater,  $I$ , was equal to the total current minus the current through the potential divider:

$$I = V_P - \frac{V_Q}{10}$$

The energy input =  $VIt$ . The duration of energy input,  $t$ , was measured with a stopwatch to better than 0.05% accuracy. At 0°C,  $V \approx 6$  volts and  $I \approx 0.05$  amp. for the 100 ohm heater;  $V \approx 3$  volts and  $I \approx 0.12$  amp. for the 20 ohm heater. Thus the power was approximately 0.35 watts for each thermometer at 0°C, producing a temperature rise of  $\sim 0.5^\circ\text{C}$  per minute for the calorimeter vessel when containing a sample weighing 30 g.

Since the heater resistance varied with temperature, the power input varied also, and had to be averaged. The voltage,  $V$ , across the 100 ohm heater (Figure 8a) was virtually constant during one heat input, but the current changed considerably. For a  $10^\circ\text{C}$  temperature rise, the heater resistance changed by 4 ohms or one twenty-fifth of its value. Thus the current also changed by approximately this fraction. Since the battery potential =  $V + V_P = 6$ ,  $V = 6 - V_P$ .  $V_P$  was only  $\frac{1}{100}$  of  $V$ , and changed by only  $\frac{1}{25}$ , so that the change in  $V$  was  $\frac{1}{2500}$  or 0.04% for one heat input.

For the strain-free heater (Figure 8b), the circuit was arranged so that the power input remained approximately constant. As the temperature rose, the heater resistance increased, and the current was lowered. Thus the voltage drop across the 20 ohm resistance of the circuit decreased, and the potential across the heater rose. Since the heater resistance was approximately the same as the 20 ohm resistance, the rise in potential across the heater approximately compensated for the lowering of current through it. (See Appendix V for power change calculations).

(ii) Temperature Measurement: (Figure 8)

The temperature was calculated from the resistance of the thermometer, which was found by comparing with a standard. The potentials across the thermometer,  $V_Q$ , and across a standard 10 ohm resistance,  $V_P$ , were measured for the 100 ohm thermometer. Since the currents were the same through each resistance, the thermometer resistance,

$$R_t = \frac{10 V_Q}{V_P}$$

With the 20 ohm thermometer, a 20 ohm standard resistance was used, so that

$$R_t = 20 \frac{V_Q}{V_P}$$

Because the four lead type of thermometer was used, the measurements were independent of lead wire resistances.

A current of 1.2 milliamperes was used for the 100 ohm thermometer and 0.6 milliamperes for the 20 ohm thermometer. These relatively high currents reduced the effect of parasitic thermal e.m.f.'s in the circuit, while apparently causing negligible heating. The power generated by the current for the 100 ohm thermometer was  $1.4 \times 10^{-4}$  watts ( $7 \times 10^{-6}$  w for the 20 ohm thermometer). This was  $3 \times 10^{-4}$  as much power as used when heating the calorimeter vessel.

The resistance measurements were reproducible to 0.01%, which corresponded to 0.02°C near 0°C.

### III. CALIBRATION AND PERFORMANCE

#### 1. Calibration of Resistance Thermometer

##### a. Fixed Points:

The resistance thermometers were calibrated at International Temperature

Scale fixed points.<sup>9</sup> The calibration points were:

Basic fixed points:

- (i) The temperature of equilibrium between liquid and gaseous oxygen at the pressure of one standard atmosphere (760 mm. of Hg):

Oxygen point      -182.97°C

- (ii) The temperature of equilibrium between ice and air saturated water at normal atmospheric pressure:

Ice point            0.000°C

- (iii) The temperature of equilibrium between liquid water and its vapour at the pressure of one standard atmosphere:

Steam point         100.000°C

Secondary fixed point:

- (iv) The temperature of freezing mercury at the pressure of one standard atmosphere:

Mercury point      -38.87°C.

Although the basic sulphur point (444.60°C) is recommended for calibration, the secondary mercury point was used because of the relative ease of attaining this temperature.

b. Calibration Apparatus<sup>9</sup>

- (i) Oxygen point:

In order to standardize it at the oxygen point, the thermometer, contained in a glass tube, was immersed in liquid oxygen. The formula used to find the temperature of equilibrium between liquid and gaseous oxygen at a

pressure  $p$  (mm. Hg) is: 
$$t_p = -182.97 + 9.530 \left( \frac{p}{760} - 1 \right) - 3.72 \left( \frac{p}{760} - 1 \right)^2 + 2.2 \left( \frac{p}{760} - 1 \right)^3$$

Because of the commercial brand of liquid oxygen used and because of the uncertainty in  $p$ , the oxygen point was accurate to only  $\sim 0.1^\circ\text{C}$ .

(ii) Ice point and mercury point (see Figure 9a):

To calibrate at the ice and mercury points, the thermometer was placed in a glass tube containing acetone for fast thermal conduction. The tube was immersed in distilled water or mercury, which was contained in an evacuable Dewar flask. The flask was surrounded by a mixture of dry ice and acetone. When the temperature approached the transition point, the flask was evacuated, so that the temperature remained constant for some time at the ice or mercury point.

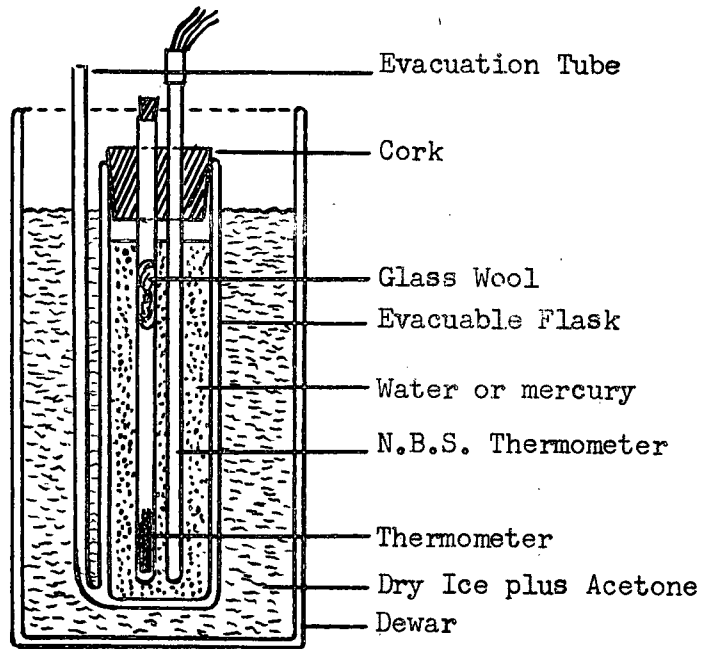
(iii) Steam point:

The steam point apparatus is shown in Figure 9b. Steam in equilibrium with water rises about the thermometer, and insulates itself from the surroundings by circulating down outside the inner tube.

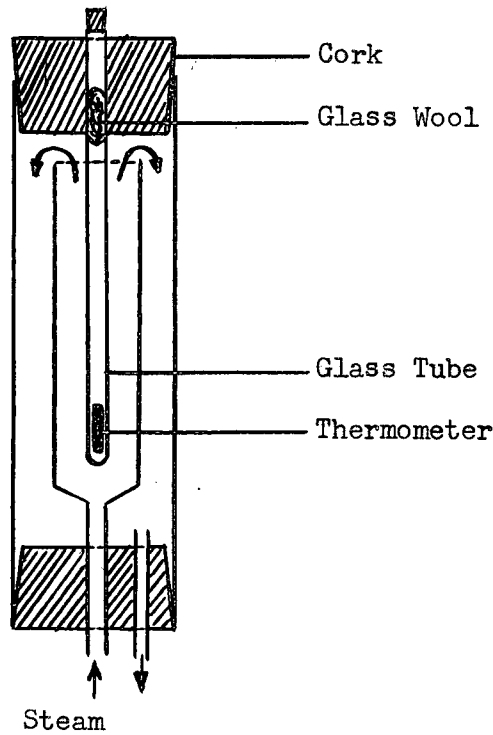
(iv) Determination of fixed points:

A Leeds and Northrup platinum resistance thermometer, calibrated by the National Bureau of Standards above  $0^\circ\text{C}$ , was used to determine the mercury and steam point temperatures. The calibration of this thermometer was checked at the ice point. Since its resistance at  $0^\circ\text{C}$  differed by only  $\sim 0.0005$  ohms from its calibrated value of 2.5117 ohms, the change was assumed to indicate a linear shift in resistance, with no change in the calibration constants,  $R_{100} - R_0$  and  $\delta$ .

The resistance of this thermometer was measured with a Leeds and Northrup Mueller dial bridge. The lead resistances were eliminated by using a mercury commutator to switch leads. For a balanced bridge (see diagram),

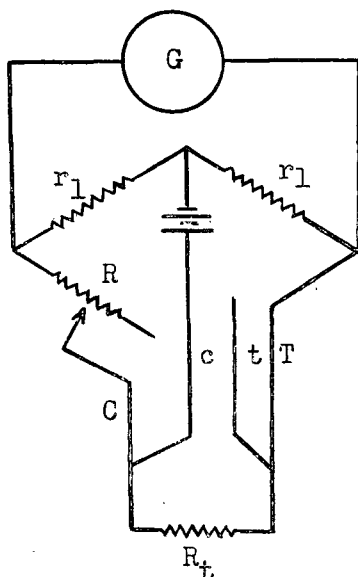


a. Ice and Mercury Point Apparatus



b. Steam Point Apparatus

Figure 9. Calibration Apparatus.



$$R_1 + C = R_t + T,$$

where  $R_1$  is the bridge reading. With  $T$  and  $C$  and  $t$  and  $c$  switched,

$$R_2 + T = R_t + C$$

$$\therefore R_t = \frac{R_1 + R_2}{2}$$

The connecting resistances of the commutator also are eliminated by

taking measurements with the thermometer resistance,  $R_t$ , shunted out.

### c. Calibration Formulae

The relation between resistance and temperature,  $t$ , of a platinum resistance thermometer for temperatures from 0 to 630°C is:<sup>8, 9</sup>

$$R_t = R_0(1 + At + Bt^2) \quad (1)$$

$R_0$  is the resistance at 0°C and  $A$  and  $B$  are constants determined by calibration at the steam and sulphur points. For temperatures from -183 to 0°C.

$$R_t = R_0 \left[ 1 + At + Bt^2 + C(t - 100)t^3 \right] \quad (2)$$

The additional constant,  $C$ , is determined by calibration at the oxygen point.

For these ranges, the temperatures found from these formulae, using a standard platinum resistance thermometer, represent the International Temperature Scale. The first equation is equivalent to Callendar's equation:

$$t = \frac{R_t - R_0}{R_{100} - R_0} 100 + \delta \left[ (0.01 t)^2 - 0.01 t \right] \quad (3)$$

$$\text{where } \delta = - \frac{10^4 B}{A + 100B}$$

(See Appendix VI).

The second equation is equivalent to:

$$t = \frac{R_t - R_0}{R_{100} - R_0} 100 + \delta \left[ (0.01 t)^2 - 0.01 t \right] + D(t-100)t^3 \quad (4)$$

$$\text{where } D = - \frac{C}{A + 100 B}$$

(See Appendix VI).

These formulae enable the temperature to be easily calculated from the resistance by a successive approximation method. The first approximation,

$$t_1 = \frac{R_t - R_0}{R_{100} - R_0} 100$$

The second approximation is attained by substituting  $t_1$  in the right hand side of equation (4),

$$\begin{aligned} t_2 &= t_1 + \delta \left[ (0.01 t_1)^2 - 0.01 t_1 \right] + D(t_1 - 100)t_1^3 \\ &= t_1 + f(t_1) \end{aligned}$$

The third approximation,  $t_3 = t_1 + f(t_2)$ , and so on. In practice,  $t_2$  can be estimated, so that only one calculation need be made to find the final approximation,  $t_3$ .

#### d. Calibration Results

##### (i) Commercial thermometer:

The first calibration of the commercial 100 ohm thermometer gave the following results:

Oxygen point	$R_{-182.9} = 24.740$ abs. ohms	
Mercury point	$R_{-38.84} = 84.725$	
Ice point	$R_0 = 100.24$	(5)
Steam point	$R_{100} = 139.02$	

The temperature of the mercury point was found from the Leeds and Northrup thermometer resistance at that point.

The value  $R_{100}$  was calculated using the Leeds and Northrup thermometer, whose calibration constants were  $R_0' = 2.5117$ ,  $R_{100}' - R_0' = 0.9732$ , and  $\delta' = 1.502$ . At the steam point, the resistance of the Leeds and Northrup thermometer was  $R_t' = 3.4844$ . Thus, using equation (3), the temperature,

$$t = \frac{3.4844 - 2.5117}{0.9732} 100 + (\text{a negligible quantity}) = 99.95^\circ\text{C}.$$

at which  $R_t = 139.00$  for the commercial thermometer.

Since  $R_0 = 100.24$ ,

$$R_{99.95} - R_0 = 38.76$$

To find  $R_{100}$ :

$$\text{SR for } 0.05^\circ\text{C is } \frac{38.76}{99.95} \times 0.05 \times 0.985 = 0.019,$$

where 0.985 is the value of  $\frac{\Delta(\text{pt})}{\Delta t}$  (and  $\text{pt} = \frac{R_t - R_0}{R_{100} - R_0} 100$ )

near  $100^\circ\text{C}$  for a thermometer with  $\delta = 1.50$ .

Therefore  $R_{100} = 139.00 + 0.019 = 139.02$

$$R_{100} - R_0 = 38.78 \text{ abs. ohms.}$$

The resistances obtained by calibration (equation (5)) were substituted in equation (2) to find the constants:

$$A = 3.952 \times 10^{-3}$$

$$B = -8.38 \times 10^{-7}$$

$$C = -1.3 \times 10^{-12}$$

Thus  $\delta = 2.17$

and  $D = 3.4 \times 10^{-10}$

Equation (4) becomes:

$$t = (R_t - 100.24) 2.5786 + 2.17 \left[ (0.01 t)^2 - 0.01 t \right] + 3.4 \times 10^{-10} (t - 100)t^3$$

After this commercial thermometer had been used for temperatures from -150 to 150°C, it was recalibrated. The results were:

$$R_{-38.87} = 84.65$$

$$R_0 = 100.06$$

$$R_{100} = 138.91$$

therefore  $R_{100} - R_0 = 38.85$

and  $\delta = 1.47$

therefore  $t = (R_t - 100.06) 2.5740 + 1.47 \left[ (0.01 t)^2 - 0.01 t \right]$

for  $0 < t < 630^\circ\text{C}$ .

The calibration of the thermometer had changed considerably. The change caused an appreciable error in temperature interval measurements, which increased as the temperature differed more from 0°C.

(ii) Strain-free thermometer:

The calibration of the strain-free thermometer gave the following results:

$$R_{-183.0} = 4.491$$

$$R_{-38.87} = 15.390$$

$$R_0 = 18.218$$

$$R_{100} = 25.348$$

From these,  $R_{100} - R_0 = 7.130$

$\delta = 1.46$

and  $D = 1.14 \times 10^{-9}$

Thus, 
$$t = (R_t - 18.218) 14.025 + 1.46 [(.01 t)^2 - .01 t] + 1.14 \times 10^{-9}(t - 100)t^3$$

After the thermometer had been used from -100 to 150°C, its zero point was checked and was found to be the same within 0.001 ohm.

## 2. Heat Capacity of the Calorimeter

The calorimeter was calibrated by measuring its capacity when it contained a standard substance. This method was preferable to calibrating the empty calorimeter, because conditions were closer to those achieved when the calorimeter contained a specimen. Of the heat capacity standards recommended,<sup>15</sup> aluminum oxide was chosen because of its availability and stability. Electrically fused crystalline carbon-free alumina (RR Alundum), produced by Norton Co., Mass., was used.

The calibration results for low temperatures, obtained using the commercial thermometer, are shown in Tables I and II and Figure 10. It is seen that, as expected from the behaviour of copper, the heat capacity of the calorimeter decreased rather rapidly below 0°C. Since the capacity at temperatures above 0°C was found from preliminary measurements to be approximately constant, it was assumed to increase only from 15.8 j/°C at 0°C (see Figure 10) to 15.9 j/°C at 100°C.

## 3. Accuracy of Specific Heat Measurements.

The accuracy of results and consistency of performance of the adiabatic calorimeter are limited by certain errors inherent in the apparatus:

Table I

Measured Capacities of Calorimeter

Plus Aluminum Oxide

(Plotted in Figure 10)

Weight of Calorimeter = 42.26 g.    Weight of  $\text{Al}_2\text{O}_3$  = 19.91 g.

(Temperature intervals varied from 11 to 15°C.)

<u>Average Temperature</u> (°C)	<u>Capacity</u> (j/°C.)
-92.8	22.9
-80.6	24.2
-60.4	26.3
-60.0	26.1
-46.1	27.2
-33.3	28.3
-21.4	28.9

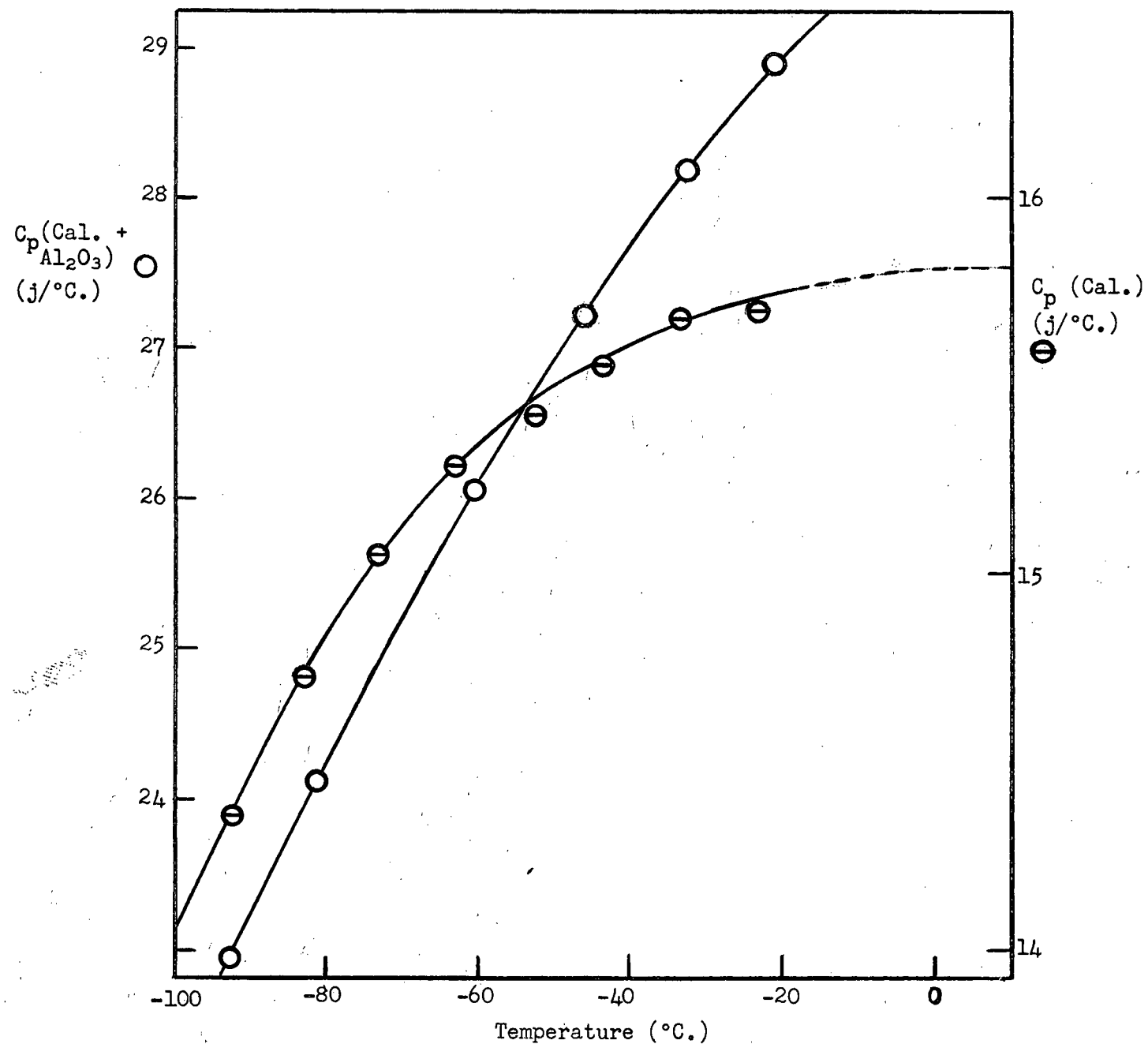


Figure 10. Heat Capacities of Calorimeter and of Calorimeter plus Alumina.

Table IICalorimeter Capacity

(Capacity of calorimeter plus  $\text{Al}_2\text{O}_3$   
obtained from Figure 10)

(Plotted in Figure 10)

Weight of Calorimeter = 42.26 g.

Weight of  $\text{Al}_2\text{O}_3$  = 19.91 g. = 0.1953 moles

T°K	$\text{Al}_2\text{O}_3$ $C_p$	Cal. + $\text{Al}_2\text{O}_3$ $C_p$	Cal. $C_p(\text{J}/^\circ\text{C})$
180	8.55	22.93	14.38
190	9.28	24.02	14.74
200	9.99	25.05	15.06
210	10.66	25.95	15.29
220	11.31	26.75	15.44
230	11.93	27.50	15.57
240	12.52	28.20	15.68
250	13.09	28.80	15.71

a. Thermal Leakage Error

Since for any calorimeter heat is transferred between the calorimeter vessel and its surroundings, an error in accounting for this heat transfer is involved. In an adiabatic calorimeter, the heat transfer is not calculated, but is reduced to a minimum. The resulting error in temperature of the calorimeter is :

$$\eta = \phi kt ,$$

where  $\phi$  is the thermal head or the difference in temperature between the calorimeter vessel and shield, k is the leakage modulus and t is the length of time for which the thermal head occurs.

The maximum error,  $\eta_{\max} = \phi_{\max} kt$ , if  $\phi_{\max}$  is the maximum thermal head for the time t..

For this adiabatic calorimeter, the thermal leakage modulus was measured for various temperatures and pressures by controlling the thermal head by means of the adiabatic shield controls. The resulting values (for a 30 g. sample in the calorimeter vessel) were:

Temperature (°C.)	-70	-20	-20
Pressure (microns)	0.2	0.1	0.5
k (°C/min./°C head)	.01	0.015	0.02

Temperature	20	20	40	40	100	100	140
Pressure	0.15	2	0.2	0.5	0.1	3	0.3
k	0.015	0.06	0.012	0.03	0.025	0.07	0.04

(See Figure 11)

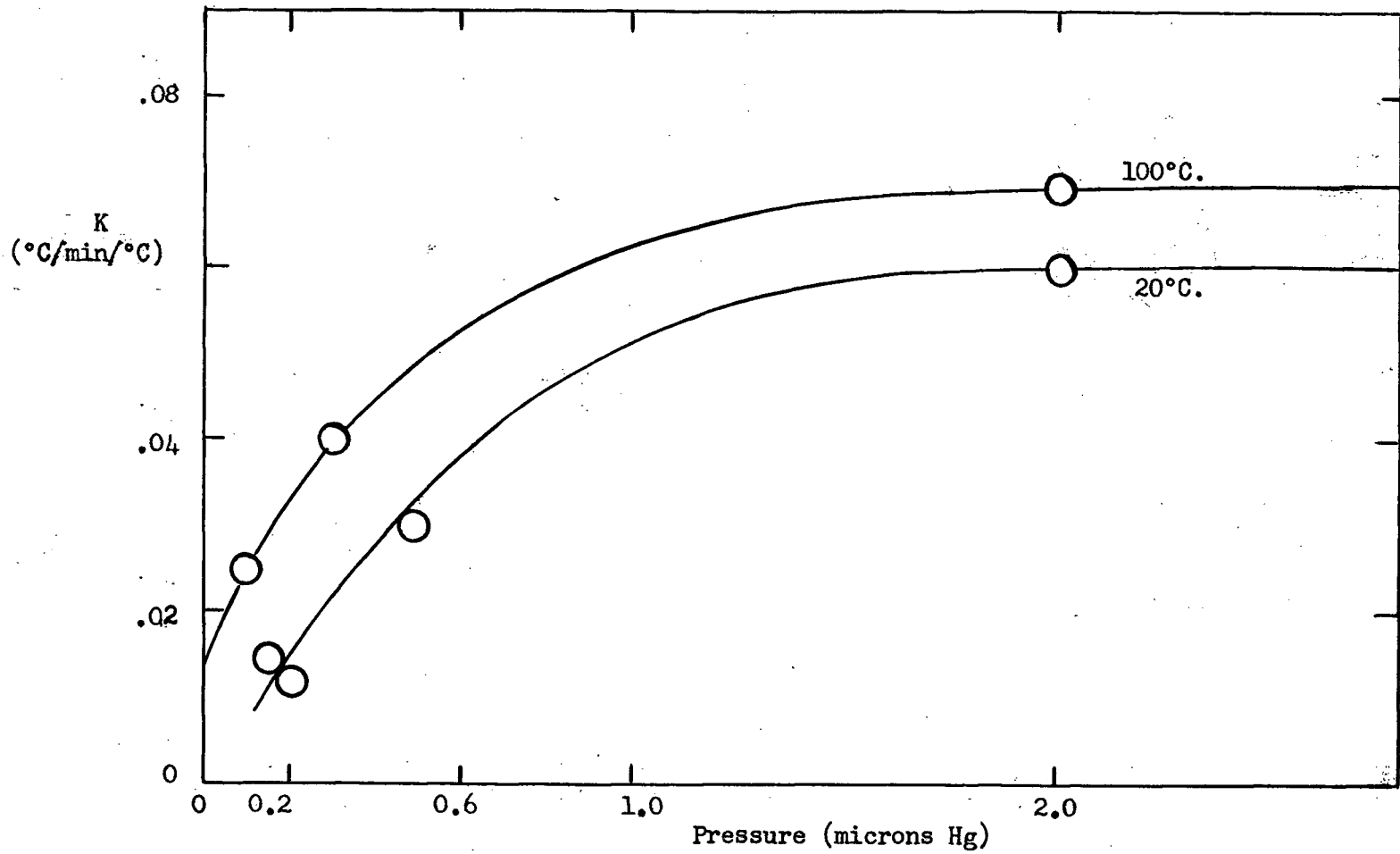


Figure 11: Variation of Thermal Leakage Modulus,  $K$ , with Pressure.

For a thermal head between calorimeter and shield bottom only:

Temperature (°C.)	50
Pressure ( $\mu$ )	0.2
$k_b$ (°C/min./°C)	0.004

A Philips ionization gauge, calibrated with a McLeod gauge, was used to measure the pressures. As can be seen by the Tables and Figure 11, the thermal leakage modulus increases only slightly with temperature, but greatly with pressure up to about one micron of mercury.

The lowest pressure obtained with this calorimeter was about 0.1 micron, because of the volatiles present (mainly the insulating varnish). As the thermal head between the shield and outer case increased, and thus the shield current increased, the pressure from the volatiles multiplied. Thus with this thermal head a minimum (less than 50°C), the least thermal leakage was obtained because of the low pressure, and also because of the ease of controlling the shield temperature.

The maximum error in temperature arising from thermal leakage can be calculated from the formula noted previously:

$$h_{\max} = \phi_{\max} kt$$

For a 10°C temperature rise, heat was supplied to the calorimeter vessel for about 20 minutes, and an equilibrium period of 5 to 10 minutes was required. Thus  $t = 30$  minutes. If  $\phi_{\max} = 1^\circ/10^\circ\text{C}$ , and  $k = 0.03^\circ\text{C}/\text{min.}/^\circ\text{C}$ , then  $h_{\max} \approx 0.1^\circ\text{C}$ . Consequently, the maximum error in temperature interval would be 1%. Since  $\phi$  will average much less than its maximum, the error from this source will be much less than 1%. With careful shield control,  $\phi$  could be kept within  $1^\circ/30^\circ\text{C}$ , and the resulting maximum possible error would be 0.3%. The probable thermal leakage

error (the mean value of a random selection of positive errors) would then likely be less than 0.1%.

Besides the thermal leakage caused by a thermal head measurable with the thermocouples, there can be leakage by other means, such as by conduction along leads and by radiation from hot spots. This leakage causes the calorimeter vessel temperature to drift linearly with time. However, this effect was usually negligible for this calorimeter if the shield temperature was within 50°C. of the outer case temperature.

b. Energy Input Error

Since the resistance of the thermometer-heater varied considerably with temperature, the power supplied by the heater also changed. The averaging of this power introduced an error in the energy input measurement.

The voltage across the commercial 100 ohm thermometer remained almost constant during a heat input, but the current decreased by  $\sim 4\%$  for a ten degree temperature rise (see Section II, 2f). The decrease in current was not uniform. It was rapid as the power input was started and quick local heating occurred, but after one or two minutes it became uniform as the heating rate became more constant. In order to average the current, it was measured at one to two minute intervals. The averaging process introduced a maximum error of 0.1% in the total energy input measurement.

The circuit for the strain-free 20 ohm thermometer was arranged so that the power remained almost constant (see Section II, 2f). The theoretical power change for a 10°C temperature rise is 0.05% if the initial heater resistance is equal to the resistance of the rest of the circuit (see Appendix V). In practice, the power change resulting from a 10°C temperature rise was about

0.5% near 0°C. The error involved in averaging the power was thus about 0.05%.

An additional error in power input measurement resulted from inaccuracies in potentiometer readings. This error amounted to  $\sim 0.05\%$ . The total maximum error in measurement of the energy input was thus  $\sim 0.1\%$ .

c. Temperature Measurement Error.

The largest error in specific heat calculations (as is usually the case in calorimetry) was caused by inaccurate temperature measurement. Errors in temperature as measured by a platinum resistance thermometer may be caused by:

- (i) Inaccurate calibration or change in calibration of the thermometer:

Uncertainties in the thermometer calibration cause errors in the temperature measurement, and consequently in the temperature interval measurement. The latter must be the more accurate; although a temperature error of 0.5°C is not serious, a 0.1°C error in the temperature interval is rather large, since it causes a 1% error in specific heat if the temperature interval is 10°C. Fortunately, errors caused by calibration deviations tend to cancel out for temperature differences, so that they are not so serious as might be supposed.

Errors caused by inaccurate calibration are not large, because the calibration must be very poor to produce significant errors (see Appendix VII). Moreover, these errors will not vary with time, and will change gradually with temperature, so that their effect on specific heat anomalies will be small.

Changes in the calibration constants of the thermometer, caused by strains or impurities in the platinum, are more serious. The error in temperature interval caused by the measured changes in calibration of the commercial thermometer was  $\sim 0.1^\circ\text{C}$  for a 10°C interval near 100°C (see Appendix VII). Although this error was large, its effect on the specific heat anomaly was reduced

because of its gradual change with temperature.

Errors resulting from calibration deviations were greatly reduced by using the strain-free thermometer, whose calibration constants remained very steady.

(ii) Inaccurate resistance measurement:

The greatest error in temperature measurement for the strain-free thermometer was caused by the error in potentiometer readings. The potentiometer was accurate to 0.01%. Since the thermometer resistance was found from the quotient of two potentiometer measurements (see Section II, 2f), the maximum error in the resistance was 0.02%, which corresponded to a temperature error of 0.05°C. The maximum error in the temperature interval was then 0.1°C, but the probable error was considerably less, approximately 0.015°C. In a 10°C temperature interval, this produced an interval error of 0.15%.

As the maximum error was considerably greater than this, a more accurate means of measuring the thermometer resistance would have been desirable. A more accurate potentiometer could be used. Some form of Wheatstone bridge circuit is often used; a Mueller bridge is perhaps the most accurate one available, giving precision up to 0.001°C.

The total error in specific heat measurement for this calorimeter, under adequate working conditions and using the strain-free thermometer, was thus made up of probable errors of a 0.1% thermal leakage error, a 0.05% power measurement error, and a 0.15% temperature measurement error. The total maximum error was ~ 1.5% and the probable error was ~ 0.2%. However, the accuracy of the calorimeter is perhaps best described by an error which is not likely to be exceeded. If an error is used which only five percent of a random sample of errors

exceeds, the accuracy was  $\sim 0.5\%$ . For all practical purposes, this is a suitable value to use, so that the accuracy of the specific heat measurements was  $0.5\%$ .

#### IV. RESULTS

##### 1. Preparation and Properties of Alloys.

###### a. Preparation of Alloys:

Alloys close to the compositions  $Mn_3AlC$  and  $Mn_3ZnC$  were prepared.

The materials used were:

Mn: 99.9% purity, donated by the Electromanganese Corp. of America.

Al: 99.99% purity, donated by the Aluminum Co. of Canada.

Zn: 99.99% purity, donated by the Consolidated Mining and Smelting Co. of Canada.

C : spectroscopic grade.

The alloy  $Mn_3AlC$  was prepared by induction melting under an argon atmosphere in an alumina crucible. The chill cast alloy was homogenized in an evacuated silica tube for 72 hours at  $1000^\circ C$ .

The alloy  $Mn_3ZnC$  was sintered, using components  $Mn_3C$  and zinc, for three days at  $550^\circ C$  in an evacuated silica tube containing little free volume. It was then ground and resintered for 12 days at  $600^\circ C$ .

###### b. Properties of the Alloys:

###### (i) $Mn_3AlC$ :

The alloy  $Mn_3AlC$  was metallic and brittle, but easily corroded in humid conditions. X-ray powder photographs showed the alloy to be about 98% the ordered face-centered cubic phase expected, with parameter  $3.876 \text{ \AA}$ .

The saturation magnetization,  $\sigma$ , in a magnetic field of 16,000 oersteds was measured from -160 to 20°C. (113 - 293°K), using a Sucksmith ring balance. The behaviour (Figure 12) was that of a ferromagnetic substance. The Curie point, obtained by plotting  $\sigma^2$  against temperature and extrapolating the straight line to  $\sigma = 0$ , was  $\theta = 286^\circ\text{K} = 13^\circ\text{C}$ . The saturation magnetization at 0°K, obtained by plotting absolute temperature squared against  $\sigma$ , and extrapolating to zero temperature, was  $\sigma_0 = 102$  ergs/g/oersted, which corresponds to 1.2 Bohr magnetons per manganese atom. (The same value was obtained by previous researchers<sup>4</sup>).

(ii)  $\text{Mn}_3\text{ZnC}$ :

The alloy  $\text{Mn}_3\text{ZnC}$  was in powdered, non-metallic, easily-corroded form. X-ray powder photographs showed the alloy to be > 95% the ordered face-centered cubic structure expected. Two alloys were used:

Alloy 1: The first was the same alloy on which neutron diffraction measurements were made. The X-ray photograph indicated a small amount ( $\sim 2\%$ ) of a second phase. The main phase had lattice parameter:  $3.9228 \text{ \AA}$ .

Alloy 2: A large alloy of 70 grams was sintered in order to make specific heat measurements more accurate. About 5% of a second phase was present even after resintering. The lattice parameter of the cubic structure was  $3.9233 \text{ \AA}$ .

The variation of saturation magnetization with temperature for the two alloys is shown in Figure 13. The maxima were 82.6 and 80.7 erg/g/oersted for alloys 1 and 2, occurring at  $-45 (\pm 2)^\circ\text{C}$  or  $228 (\pm 2)^\circ\text{K}$ . Extrapolating the curve to 0°K for alloy 1 gave a magnetization at absolute zero which corresponded to a Bohr magneton value of one per Mn atom (see Section I, 2). Extrapolating the part of the curve above  $-45^\circ\text{C}$  to 0°K gave a value of  $\sim 1.5$  Bohr magnetons per Mn atom. These results agree within experimental error with those obtained

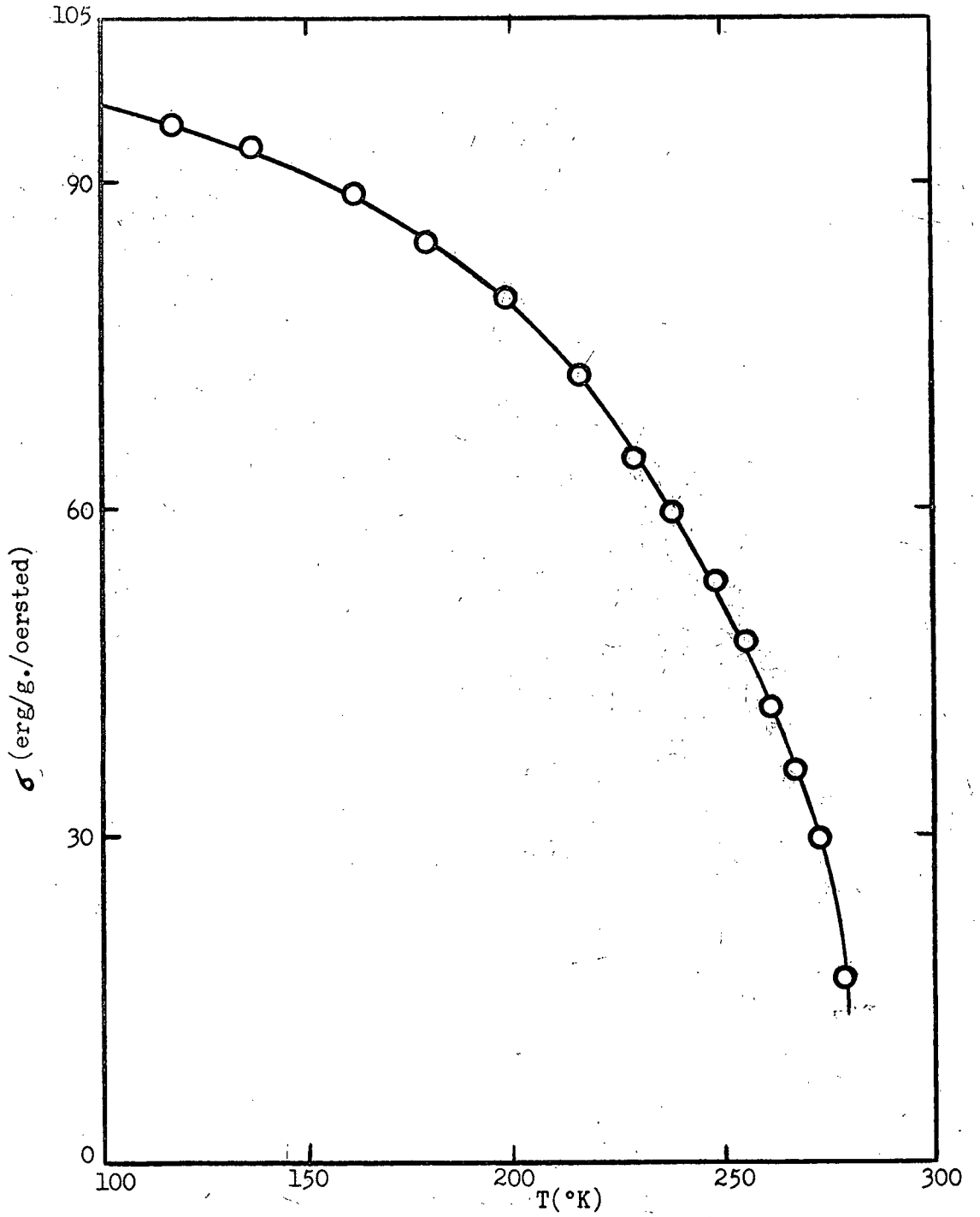


Figure 12. The Variation of Saturation Magnetization,  $\sigma$ ,  
with Temperature, T, for Mn<sub>3</sub>AlC.

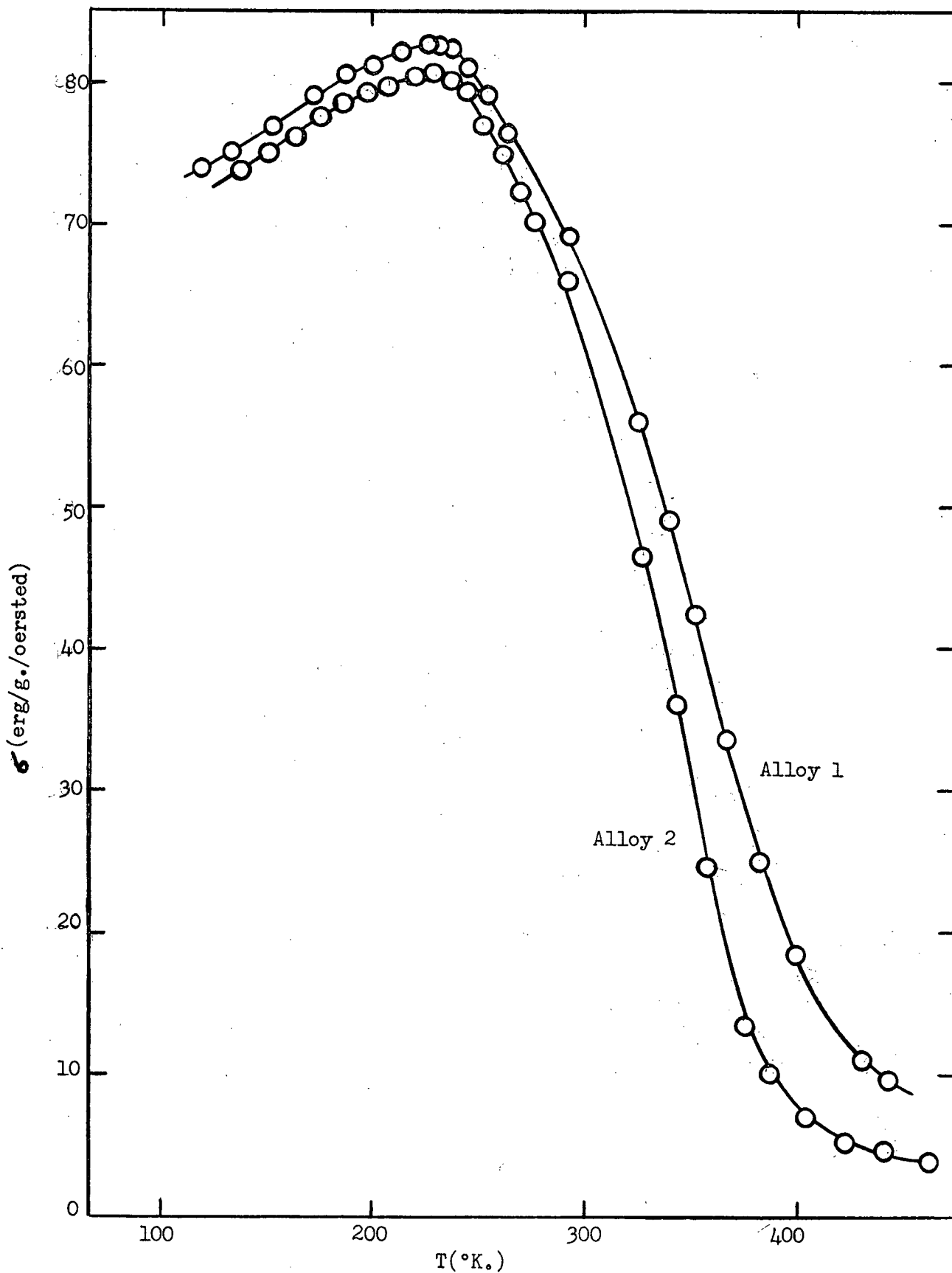


Figure 13. The Variation of Saturation Magnetization,  $\sigma$ , with Temperature,  $T$ , for  $Mn_3ZnC$ .

previously<sup>5</sup> (see Figure 2). The Curie temperatures of alloys 1 and 2 were

$\theta_1 = 391^\circ\text{K} = 118^\circ\text{C}$  and  $\theta_2 = 368^\circ\text{K} = 95^\circ\text{C}$  in a field of 16,000 oersted.

## 2. Specific Heat Measurements

### a. The Specific Heat of Mn<sub>3</sub>AlC:

The specific heat of Mn<sub>3</sub>AlC was measured from -140 to 100°C., using the commercial thermometer. The capacities of the alloy plus calorimeter are plotted in Figure 14 and are listed in Table III. The capacity of the alloy alone, obtained by using the calorimeter calibration curve of Figure 10 (Section III, 2), is plotted in Figure 15.

The specific heat curve of Mn<sub>3</sub>AlC showed the expected ferromagnetic anomaly at the Curie point, and its shape was close to that predicted by Weiss (Section I, 1). This anomaly occurred at  $-10 \pm 2^\circ\text{C}$ , which is the Curie temperature in zero magnetic field of the alloy - the Curie temperature obtained by magnetic measurements in a field of 16,000 oersteds was of course higher (13°C).

The size of the specific heat anomaly was considerably smaller than expected for an alloy of magnetization 1.2 Bohr magnetons per manganese atom. According to the Weiss theory, the height of the anomaly for a ferromagnetic substance of magnetization  $n\mu_B$  per atom is  $3n\mu_B$  cal/°C/g atom.<sup>1</sup> But the height of the Mn<sub>3</sub>AlC anomaly was  $\sim 2.2$  j/°C for 0.157 moles, or  $\sim 1.1$  cal/°C/g atom of Mn, which would correspond to only 0.37 Bohr magnetons per Mn atom. The greatest specific heat measured for the alloy (ignoring the anomaly) was 6.6 cal/g atom/°C, at 100°C.

The measurements were repeated for the same alloy, using the strain-free thermometer, with good general agreement in results (see Figure 16). The Curie temperature was  $-9 \pm 2^\circ\text{C}$  and the anomaly height was  $\sim 1.9$  j/°C. for 0.151 moles, or  $\sim 0.33$  Bohr magnetons per Mn atom.

Table IIICapacities of Mn<sub>3</sub>AlC (31.97 g)plus Calorimeter (42.18 g)

as measured with the Commercial Thermometer

(Temp. intervals varied from 5 to 12°C).

Average Temp. (°C)	Capacity (j/°C.)	Average Temp. (°C)	Capacity (j/°C)
-138.6	25.3	-2.0	35.1
-136.8	25.4	-0.8	34.9
-124.8	27.0	4.9	34.8
-111.7	28.5	6.2	34.9
-102.2	29.7	17.1	35.2
-97.3	30.1	26.0	35.2
-89.2	31.1	31.5	35.5
-89.1	30.8	36.2	35.6
-76.8	31.7	41.7	35.3
-61.6	33.2	43.8	35.3
-57.2	33.2	51.6	35.6
-43.4	34.1	52.8	35.5
-30.7	35.2	61.0	36.1
-17.4	36.1	62.3	35.9
-13.6	36.3	70.2	35.9
-11.0	36.3	74.2	36.0
-10.4	36.7	83.0	36.3
-8.8	36.6	91.7	35.9
-6.4	36.0	100.2	36.2

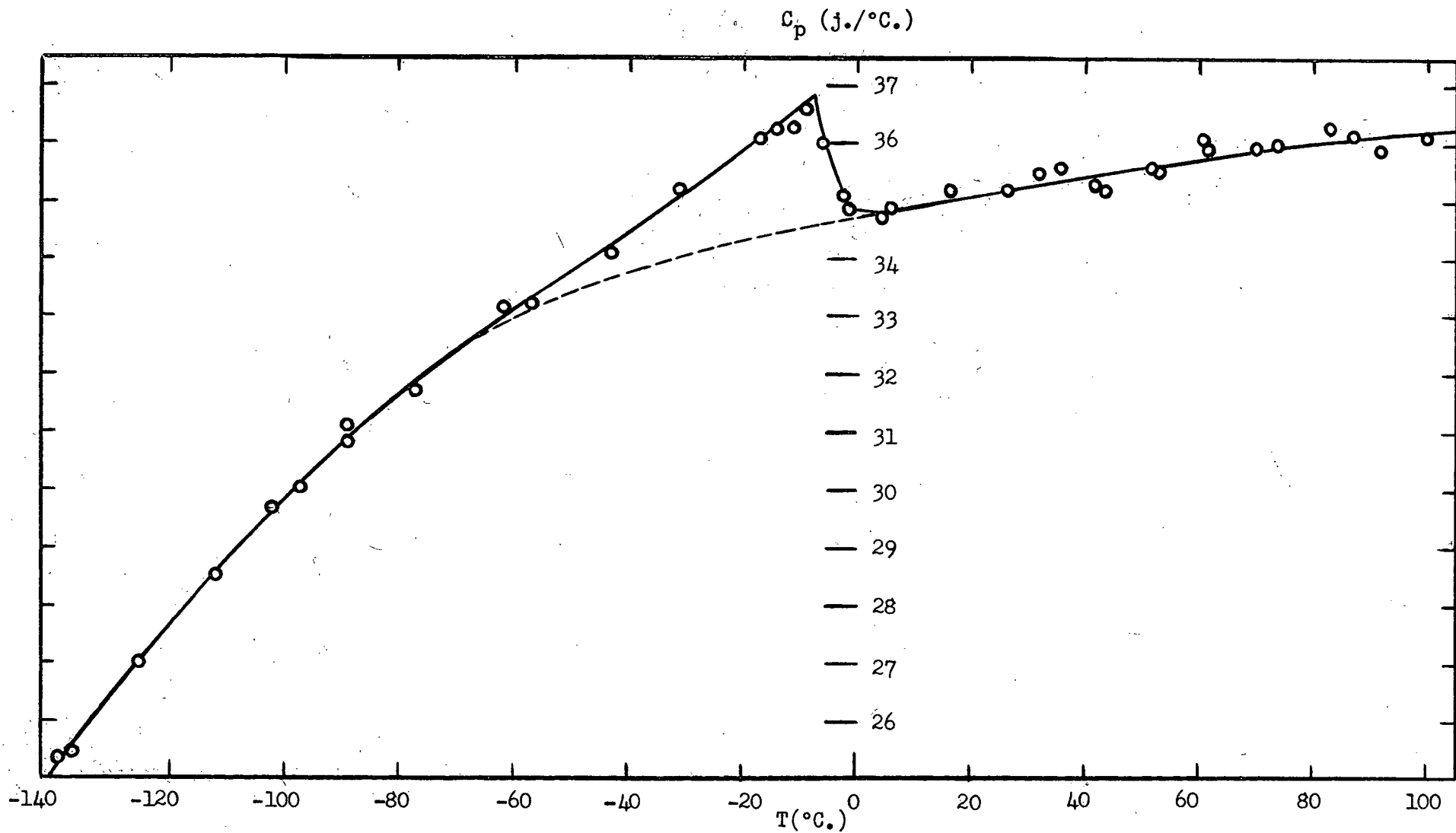


Figure 14. Capacity of  $\text{Mn}_3\text{AlC}$  Plus Calorimeter.

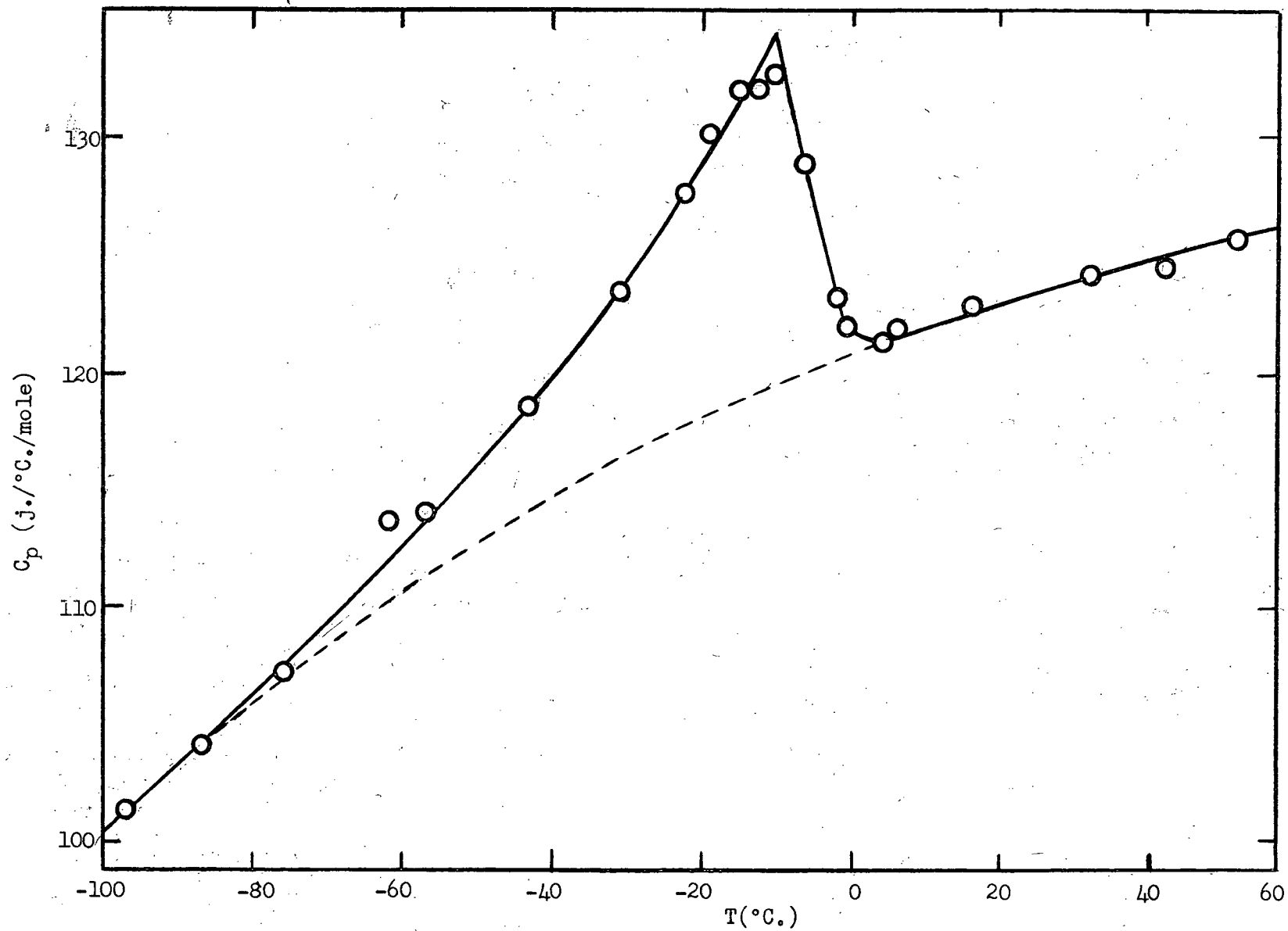


Figure 15. Capacity of  $\text{Mn}_3\text{AlC}$ .

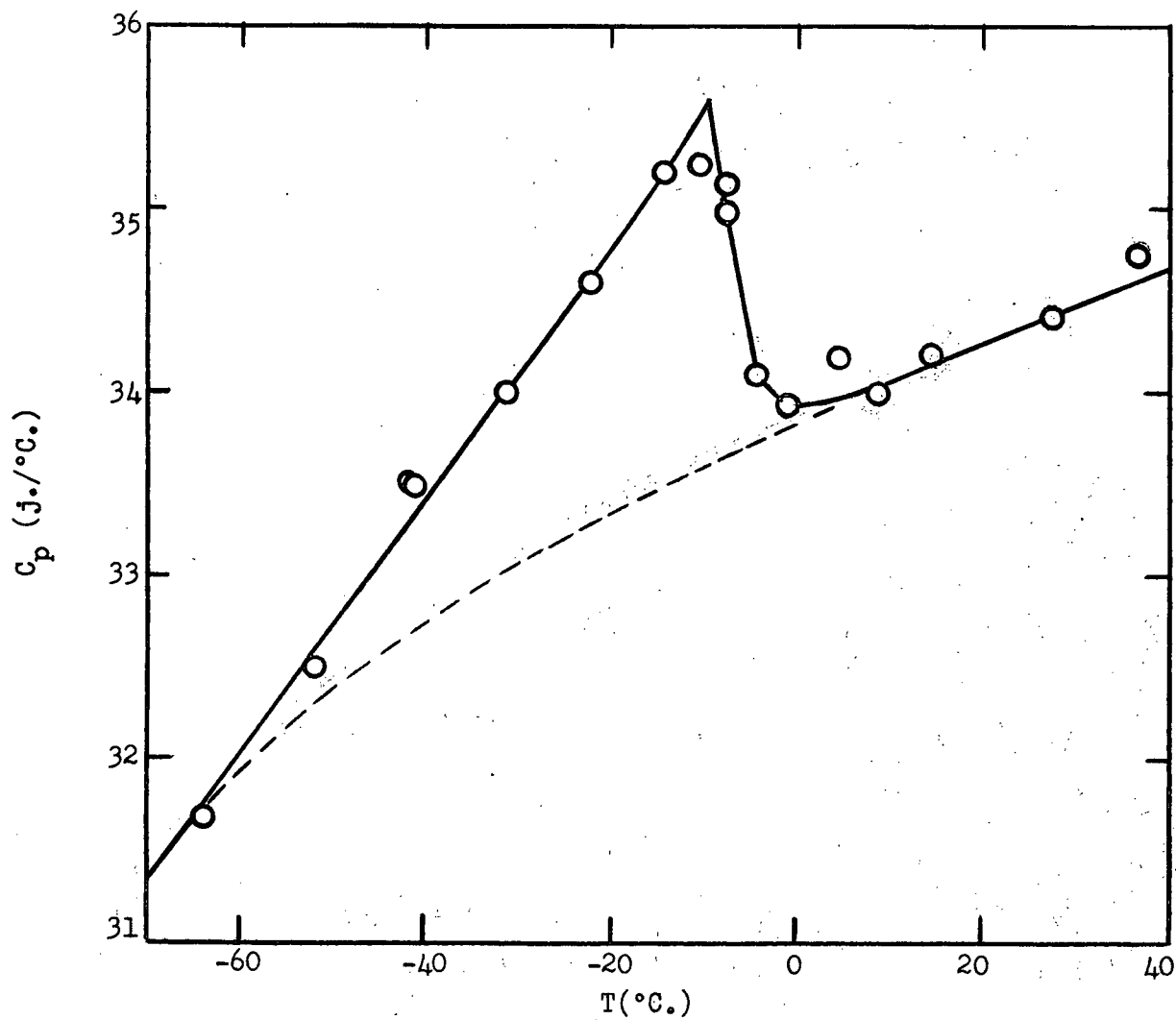


Figure 16. Capacity of  $Mn_3AlC$  + Calorimeter.  
(using the strain-free thermometer)

b. The Specific Heat of  $Mn_3ZnC$ :

(i) Alloy 1:

The heat capacity of the sample of  $Mn_3ZnC$  on which neutron diffraction measurements were made was found from  $-100$  to  $60^\circ C$ , using the commercial thermometer. The temperature intervals used were from  $8$  to  $12^\circ C$ , which were large enough to obtain accurate interval measurements, and small enough to discern sudden changes in heat capacity.

The results are shown in Figure 17. The specific heat anomaly, occurring at  $-37^\circ C$ , had the form of a normal ferromagnetic Curie point anomaly. The anomaly height was  $1.8$  j/ $^\circ C$  for  $0.083$  moles of  $Mn_3ZnC$ , or  $1.7$  cal/ $^\circ C/g$  atom of Mn. The corresponding Bohr magneton number was  $0.6$  per Mn atom. The maximum value of the specific heat reached was  $7.5$  cal/g. atom/ $^\circ C$  at  $80^\circ C$ , and at this point it was still rising quite rapidly.

(ii) Alloy 2:

Because the sample of alloy 1 was rather small, another larger sample was made, in order to increase the accuracy of the specific heat measurements. The results, obtained using the strain-free thermometer, are shown in Table IV and Figure 18. The specific heat values show two anomalies, a very sharp one at  $-35^\circ C$ , and a more rounded one at  $\sim 65^\circ C$ .

The high temperature anomaly occurred at the normal ferromagnetic Curie temperature of  $Mn_3ZnC$ . Its rounded shape was probably due to measurement errors, and possibly also due to inhomogeneity in the alloy, since the Curie temperature is very dependent on composition. The largest specific heat measured for the alloy (except for the anomaly) was  $6.8$  cal/g. atom/ $^\circ C$  at  $100^\circ C$ , which was approximately the same as that for  $Mn_3AlC$ .

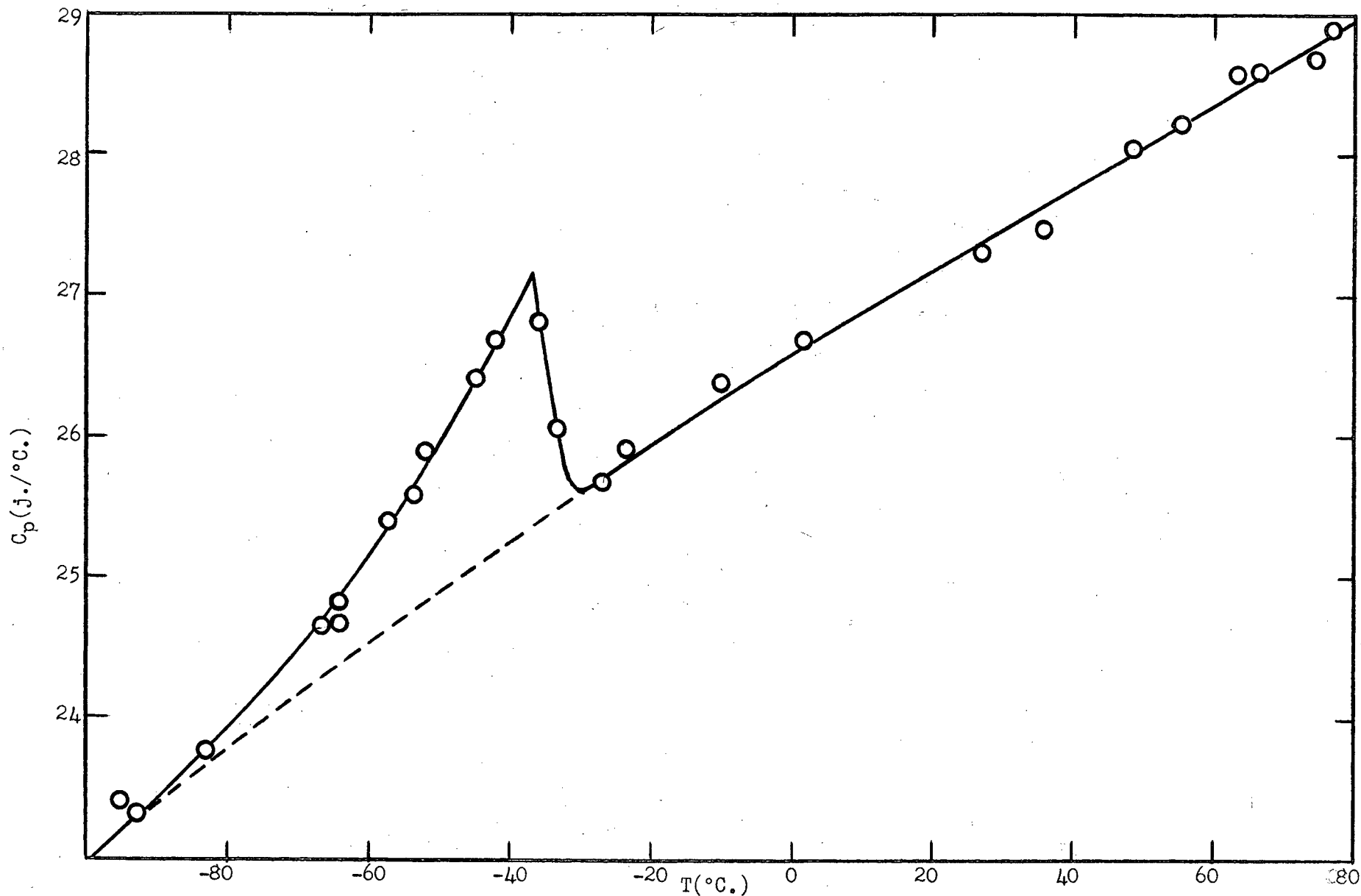


Figure 17. Capacity of  $Mn_3ZnC$  (alloy 1) plus Calorimeter

Table IV.

Capacities of Mn<sub>3</sub>ZnC (Alloy 2:51.38g.) plus Calorimeter (43.66 g.)

as measured with the Strain-Free Thermometer.

(Temperature intervals varied from 5 to 11°C.)

Average Temp. (°C.)	Capacity (j./°C.)	Average Temp. (°C.)	Capacity (j./°C.)
-69.2	40.2	39.5	46.3
-58.4	42.0	47.5	47.1
-56.7	42.1	47.8	46.4
-53.3	42.6	49.3	46.8
-48.0	44.0	56.5	46.9
-46.5	44.3	59.8	46.8
-45.7	44.6	66.0	47.0
-40.9	46.1	69.3	46.9
-38.3	47.0	72.5	46.2
-36.8	46.5	73.1	46.0
-36.1	47.3	77.3	45.7
-31.2	42.7	79.0	45.2
-28.3	42.6	82.2	45.3
-17.9	43.0	82.2	45.6
- 7.6	43.3	89.6	45.2
27.9	45.6	91.9	46.0
29.7	45.3	101.6	45.8
37.9	45.8	111.4	45.8

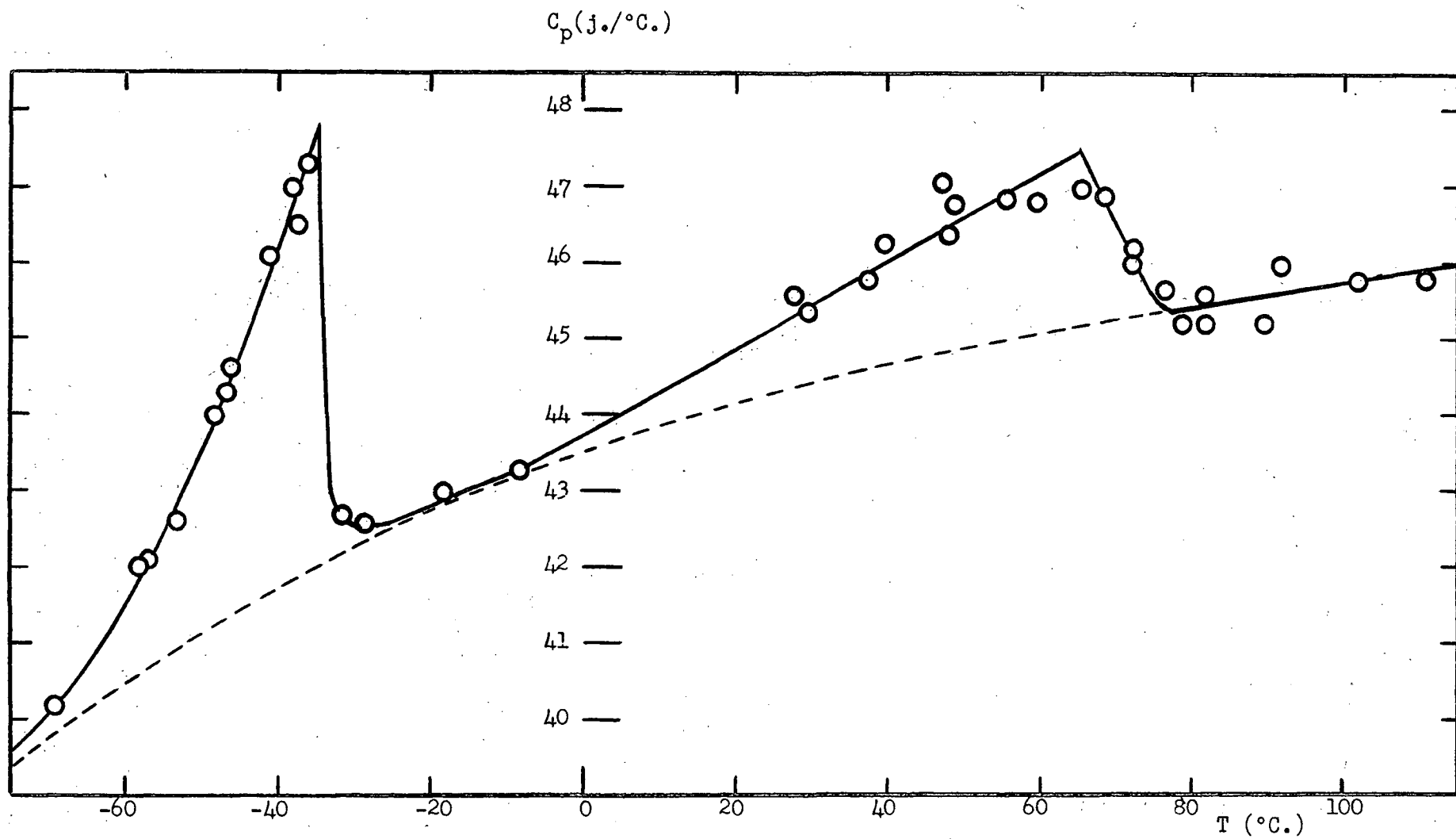


Figure 18. Capacity of  $\text{Mn}_3\text{ZnC}$  (alloy 2) plus Calorimeter.

The low temperature anomaly had a very sharp peak, dropping to zero over only about a 3°C interval. This anomaly thus was very close to the theoretical form predicted from the Weiss theory, which has a discontinuity at the Curie temperature. Such an approach to discontinuity has not been observed before. The height of the anomaly was 5.5 j/°C for 0.212 moles, or 2.1 cal/°C/g atom of Mn.

c. Magnetic Specific Heats and Entropies:

The anomalous specific heat caused by the magnetic change at the Curie point may be found by writing the observed specific heat as:<sup>16</sup>

$$C_o = C_q + (C_p - C_v) + C_i + S$$

where  $C_q$  = specific heat at constant volume from Debye theory.

$C_p - C_v$  = correction for dilatation

$C_i$  = excess over the Debye value common to most metals.

$S$  = excess caused by magnetic and other changes.

In order to use this procedure, however, measurements over a large temperature range must be made. In particular, specific heats near 0°K must be found in order to calculate the electronic and the lattice specific heats. Consequently, because of the limited temperature range of these experiments, and because of further uncertainties arising at higher temperatures, this method was not suitable.

The magnetic specific heats in the present research were thus approximately determined by extrapolating the observed specific heat curves from above and below the anomalies. The results are shown in Figures 19 and 20. In Figure 19 the magnetic specific heat  $MC_M$  of  $Mn_3AlC$  (from Figure 15) is plotted, as well as the values of  $-\sigma d\sigma/dT$  obtained from the magnetization

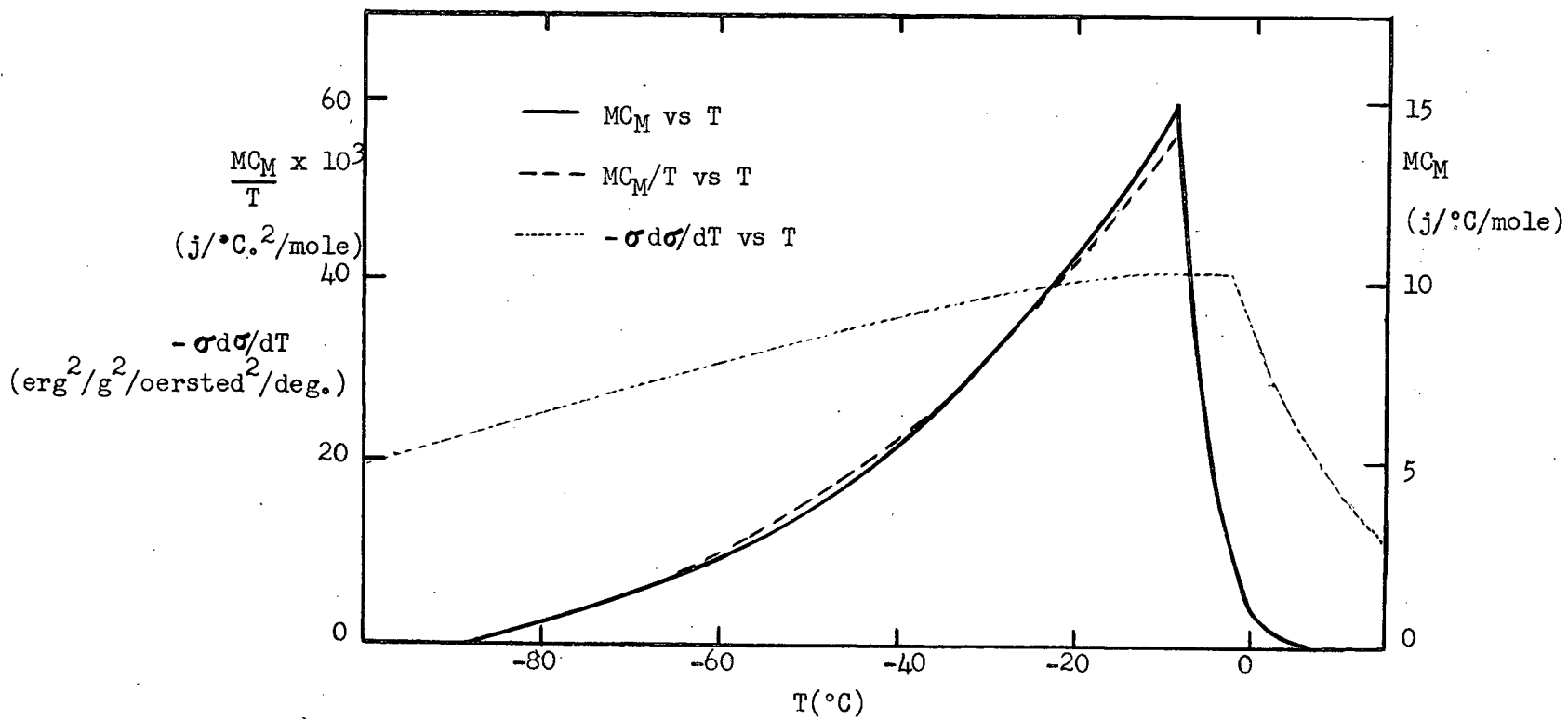


Fig. 19. Magnetic Specific Heat of Mn<sub>3</sub>AlC.

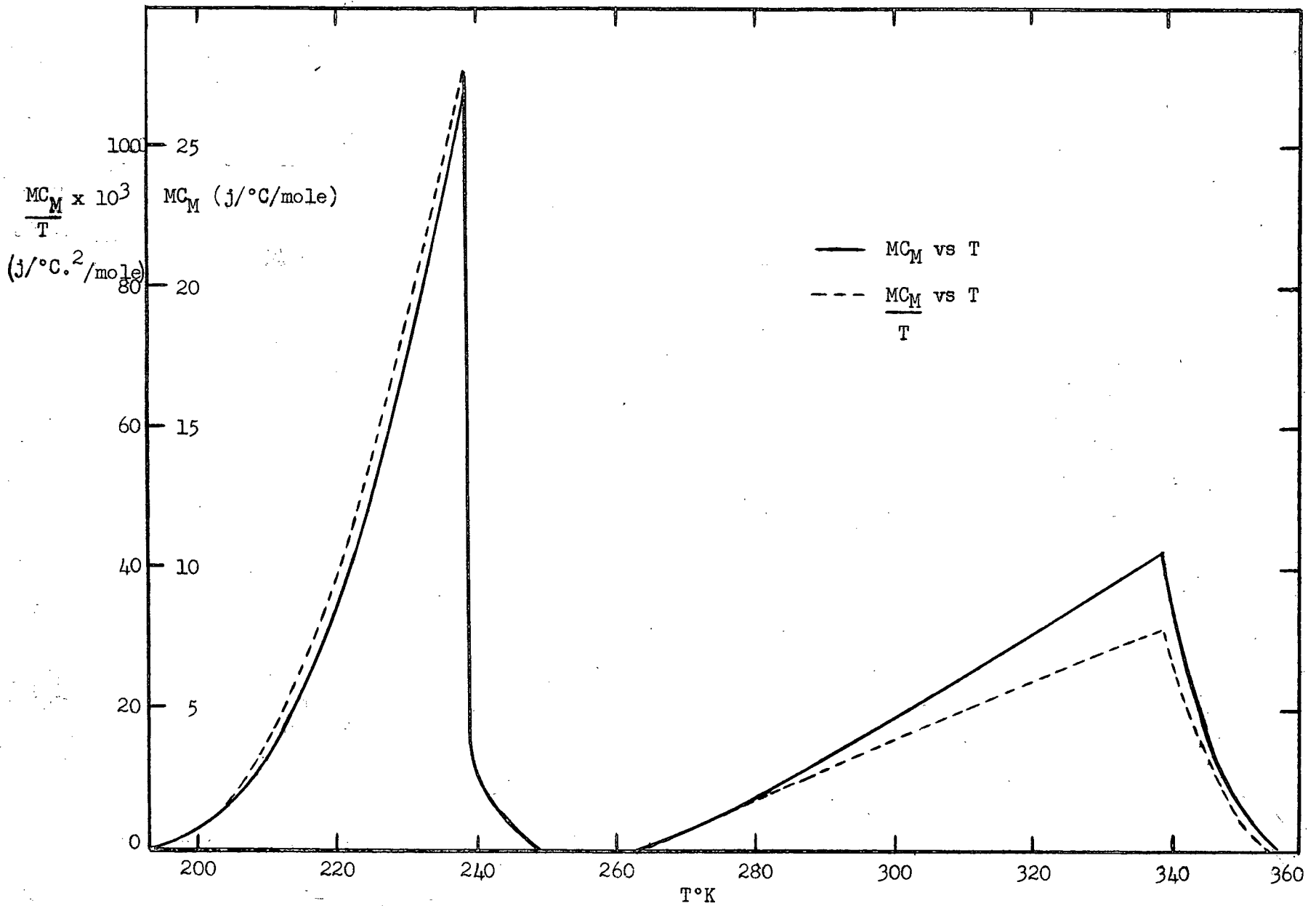


Fig. 20 Magnetic Specific Heat of Mn<sub>3</sub>ZnC (Alloy 2).

curve (Figure 12). ( $M$  = gram molecular weight,  $C_M$  = magnetic specific heat/gr.).

A curve of  $M C_M/T$  versus  $T$  is also plotted, which when integrated gives the

entropy change associated with the magnetic change:  $\Delta S = \int M C_M dT/T =$

1.8 j/mole/°K = 0.15 cal/g. atom Mn/°K. The magnetic energy,  $U = \int M C_M dT =$

460 j/mole = 37 cal/g. atom Mn.

Figure 20 shows the magnetic specific heat of  $Mn_3ZnC$  (alloy 2, from Figure 18), and a curve ( $M C_M/T, T$ ). The entropy changes corresponding to the low and high temperature anomalies respectively were  $\Delta S_1 = 1.7$  j/mole/°K = 0.14 cal/g. atom Mn and  $\Delta S_2 = 1.3$  j/mole/°K = 0.11 cal/g. atom Mn/°K. The magnetic energies,  $U_1 = 385$  j/mole = 31 cal/g. atom Mn and  $U_2 = 420$  j/mole = 34 cal/g. atom Mn.

## V. DISCUSSION AND CONCLUSIONS

### 1. Discussion of Results

The specific heat curves of  $Mn_3AlC$  showed a second order anomaly at its Curie point (-9°C), as expected for this ferromagnetic alloy. The curve for  $Mn_3ZnC$  showed second order anomalies at -35°C and at 65°C, which supported the previously discussed (Section I, 2) concept of the magnetic structure of the alloy: it is ferrimagnetic below -35°C, ferromagnetic between -35 and 65°C and paramagnetic above 65°C.

#### a. Weiss Theory:

The experimental results will be discussed in terms of existing magnetic theories. One of the first ferromagnetic theories was the phenomenological 'molecular field' theory of Weiss,<sup>19</sup> the quantum modification of which is in good agreement with experimental results. Weiss made the important assumption that the elementary magnets of a ferromagnetic substance are under

the influence of an effective magnetic field,  $H_e$ , which is the sum of the applied field,  $H$ , and the molecular field,  $NI$ , which is proportional to the magnetization,  $I$ . The proportionality constant,  $N$ , called the molecular field constant, is a measure of the exchange forces acting between the atoms of the substance. The magnetization can then be evaluated by using Boltzmann statistics in a manner analogous to the Langevin treatment of a paramagnetic gas. The magnetic moment of an atom in the quantum notation is

$$u_A = J g u_B$$

where  $J$  = the resultant angular momentum quantum number of an atom = the sum of orbital (L) and spin (S) quantum numbers.

$g$  = gyromagnetic ratio  
 = 2 for spin angular momentum only ( $\approx 2$  for ferromagnetic materials experimentally)

$u_B$  = the Bohr magneton, the magnetic moment of a single spinning electron  
 =  $eh/4\pi mc = 9.27 \times 10^{-21}$  erg/gauss.

Let  $\alpha = u_A H_e / KT$

where  $K$  = Boltzmann's constant and the effective field,  
 $H_e = H + NI$

Then the average magnetic moment of the substance,  $\bar{u}$ , is deduced from:

$$\frac{\bar{u}}{u_A} = \frac{I}{I_0} = \frac{\sum_{m=-J}^J \frac{m}{J} e^{m\alpha/J}}{\sum_m e^{m\alpha/J}}$$

where  $I_0$  = magnetic moment per unit volume at  $0^\circ K$ .

$$\text{Then } \frac{I}{I_0} = \frac{2J + 1}{2J} \coth \frac{(2J + 1)\alpha}{2J} - \frac{1}{2J} \coth \frac{\alpha}{2J}$$

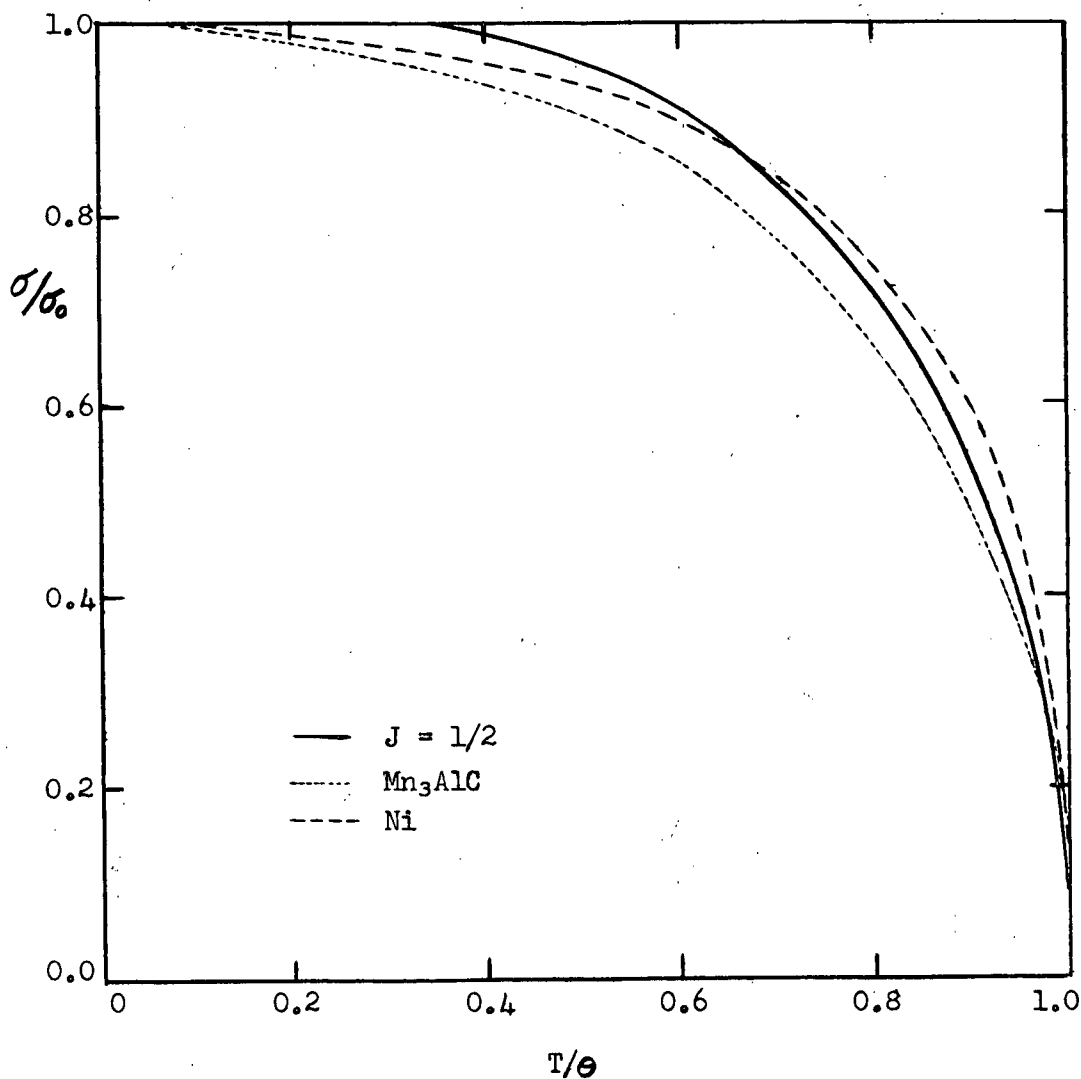


Fig. 21. Magnetization Curves, (theoretical curve for  $J = 1/2$  and experimental curves for  $Mn_3AlC$  and  $Ni$ ).

This is the Brillouin function. The Curie temperature,  $\Theta = (J+1)g\mu_B NI_0/3K$ .

For  $J = 1/2$  (a single electron spin),

$$\frac{I}{I_0} = \tanh \frac{u_A H_e}{KT} = \tanh \alpha$$

If  $H = 0$ ,  $\frac{I}{I_0} = \tanh \frac{I/I_0}{T/\Theta}$

where  $\Theta = u_A NI_0/K$

This curve agrees well with experiment.<sup>17</sup>

The saturation magnetization ( $I/I_0$ ,  $T/\Theta$ ) curve calculated for  $J = 1/2$ , and the experimental curves for Ni and  $Mn_3AlC$  are plotted in Figure 21. The calculated curve is quite close to experimental results for Ni, but differs considerably from the observed  $Mn_3AlC$  results. It should be noted that in general the curves observed for alloys are less concave to the  $T/\Theta$  axis than the curves for pure metals.<sup>20</sup> (Stoner's collective electron theory gives results close to the  $Mn_3AlC$  curve).

Using  $\Theta = u_B NI_0/K = 264^\circ K$ , the molecular field constant for  $Mn_3AlC$ ,

$$N = 6600 \text{ gauss}^2 \text{ cc/erg.}$$

The molecular field,  $NI_0 = 3.9 \times 10^6$  gauss.

For ferromagnetic  $Mn_3ZnC$ ,

$$N = 7400 \text{ gauss}^2 \text{ cc/erg.}$$

$NI_0 = 5.1 \times 10^6$  gauss, assuming the saturation moment at  $0^\circ K$  to be  $1.5 u_B$  per Mn atom.

From the Brillouin function, the molar susceptibility above the Curie point is

$$\chi_M = \frac{\sigma_M}{H} = \frac{(J+1) g u_B C_M}{3K(T - \Theta)} = \frac{C'_M}{T - \Theta}$$

The Curie constant per mole,  $C'_M = \frac{(J+1)g\mu_B^2 \sigma_{0M}}{3K}$  where  $\sigma_{0M}$  is the magnetic moment per mole with all elementary magnets aligned parallel (at 0°K). From paramagnetic data for  $Mn_3ZnC$ ,

$$N = \frac{\sigma_M}{\rho C'_M} = 2700 \text{ gauss}^2 \text{ cc/erg, where}$$

M = gram molecular weight.

This result is not very reliable because of the experimental difficulties of paramagnetic measurements (especially zinc evaporation).<sup>\*</sup> The value of  $C'_M$  could not be determined for  $Mn_3AlC$  because of the curvature of the  $(\frac{1}{X}, T)$  curve.

For best overall agreement with ferromagnetic and paramagnetic data, J is between 1/2 and 1.

The calculations of magnetic specific heat based on the Weiss theory have been summarized in Section I 1 b. The magnetic specific heat per unit mass,

$$C_M = \frac{N\mu^2}{2} \frac{d\sigma^2}{dT}$$

Then if the Brillouin function is used to evaluate  $C_M$ , the resulting specific heat anomaly rises continually with increasing temperature to the Curie point, where it drops discontinuously to zero. The form of the curve is shown in Section I 1 b. If the gyromagnetic ratio,  $g = 2$ , the magnitude of the discontinuity per gram-atom at the Curie point is  $A\Delta C_M = 3 Rn_0/2$  for  $J = 1/2$  and  $2 Rn_0$  for  $J = 1$  (where  $n_0 =$  the number of Bohr magnetons per atom and  $A =$  atomic weight).

The general form of observed magnetic specific heat anomalies is in agreement with these results.<sup>3,16,21</sup> The differences are that the observed drop at the Curie point extends over a range of temperature (from 5-100°C),

---

\* However, the values of N calculated from ferromagnetic and from paramagnetic data usually do differ considerably.

attributed to local ordering above the Curie temperature, and that the observed curves rise more rapidly than the calculated ones below the Curie point. The decreases in  $C_M$  at the Curie temperature for Fe, Co and Ni are in fair agreement with theory for  $J = 1/2$ .

Because of the difference between the theoretical magnetization curve and that observed for  $Mn_3AlC$ , the observed specific heat anomaly for this alloy can not be identical with the anomaly predicted for  $J = 1/2$ .

The values of  $\sigma d\sigma/dT$  taken from the magnetization curve for  $Mn_3AlC$  are plotted against  $T$  in Figure 19. It is seen that the resulting curve is much flatter than the  $(C_M, T)$  curve. Thus the value of the molecular field constant  $N$  in  $C_M = -N\mu d\sigma/dT$  must be changing rather rapidly over the measured temperature range. This is to be expected, since the very similar alloy  $Mn_3ZnC$  experiences a transition from ferri- to ferromagnetism in this region, which entails a reversal of sign in the molecular field.

The anomalies observed for  $Mn_3AlC$  and  $Mn_3ZnC$  (Figs. 15, 16, 18, 19, 20) were typical of magnetic anomalies reported in the literature.<sup>3,16,21</sup> The anomaly heights were  $R/2$  per Bohr magneton for  $Mn_3AlC$  and  $0.4R$  per Bohr magneton for the ferromagnetic  $Mn_3ZnC$  anomaly, as compared with the theoretical  $3 R/2$ , also observed for pure metals. The low temperature  $Mn_3ZnC$  anomaly was quite steep, indicating a rather abrupt transition from ferrimagnetism to ferromagnetism. The usually observed 'tailing off' above the transition point was absent, but was perhaps masked by the ferromagnetic anomaly.

#### b. Entropy Changes:

The total entropy associated with a ferromagnetic anomaly may be calculated from the partition function,  $Q$ , evaluated above the Curie temperature,

$$Q = \sum_{m=-J}^J e^{m\alpha/J} \quad \text{using the previously mentioned notation.}$$

The free energy,  $F = -RT \ln Q$

$$\text{The entropy, } S = \frac{-\partial F}{\partial T}$$

Thus for  $J = 1/2$  and the effective magnetic field,  $H_e = 0$  ( $T > \theta$ ),  $S = R \ln 2$  per gram-atom. In general,  $S = R \ln(2J + 1)$ .

The ferromagnetic transition may also be considered in terms of a simple model, in which each atom has one electron spin ( $S = 1/2$ ) capable of an orientation parallel or antiparallel to a given direction. At absolute zero temperature, all spins are oriented parallel, giving zero entropy. Above the Curie temperature, the electrons will represent a paramagnetic gas, with half oriented parallel and half antiparallel. Then the entropy is

$$S = K \ln \frac{N_e!}{\frac{N_e!}{2} \cdot \frac{N_e!}{2}} \quad \text{for } N_e \text{ electrons.}$$

therefore  $S = R \ln 2$  (to a good approximation for one gram-atom)

At temperatures approaching absolute zero, the magnetic specific heats (and thus the entropy changes) involved in a magnetic transition can be determined quite accurately, since the specific heats at constant pressure and at constant volume are almost identical, and the lattice specific heat is quite small. The specific heat curve for the transition from the antiferromagnetic to the paramagnetic state of  $\text{CuCl}_2 \cdot 2 \text{H}_2\text{O}$  has been found by Friedberg<sup>21</sup> to have the typical sharp peak at the transition point (4.3°K). But above this temperature it tailed off according to a  $T^{-2}$  law, probably because of short range order. The magnetic entropy change below the Néel temperature was 0.45R and in the tail was 0.20R, the sum of which is close

to the theoretical  $R \ln 2 = 0.69R = 1.4 \text{ cal/g.atom/deg.}$  expected. Similar results have been obtained for other paramagnetic salts.<sup>22</sup>

For ferromagnetic materials at elevated temperatures, the results are however far from satisfactory. The difficulty in separating the magnetic part of the specific heat is undoubtedly responsible for the error involved in calculating the entropy change. The change corresponding to the magnetic anomalies of some ferromagnetic substances has been calculated by the author from specific heat curves found in the literature. For nickel, Stoner<sup>23</sup> has used the data of several researchers to separate carefully the magnetic part of the specific heat. The corresponding entropy change was  $\Delta S = 0.5 \text{ cal/g.atom/deg.}$  ( $\Delta S = 0.3$  for only the peak of the curve, neglecting the long low temperature tail). The expected value is 0.83 if six-tenths of the atoms have  $J = 1/2$  and the rest have  $J = 0$ . If, however, as predicted by Mott and Jones<sup>24</sup>  $J = 0$  for 70 percent of the atoms and  $J = 1$  for 30 percent of them, the expected value is  $0.3 R \ln 3 = 0.66$ . This approach assumes that the individual electrons are not free in the paramagnetic state, and results from tight bonding theory. The experimental result for iron<sup>25</sup> was  $\Delta S \approx 2.0 \text{ cal/g.atom/deg.}$  The expected value is at least 2.4 (for  $J = 1$ ). These experimental values are considerably less than the theoretical, but are reconcilable with it if a rather large degree of local ordering not observed in the form of a magnetic specific heat is assumed present above the Curie temperature.

A theory of 'constant coupling' for Heisenberg ferromagnetism has been proposed by Kasteleijn and Van Kranendonk<sup>26</sup> to explain the presence of short range order above the Curie point. The entropy above the Curie point is then calculated to be  $0.31 R \ln 2$  for coordination No. 6 and  $0.12 R \ln 2$  for coordination No. 12. These values have the order of magnitude of the above mentioned discrepancies.

It is seen that even after very careful calculation of the magnetic specific heat anomaly, only qualitatively correct results for the entropy change can be obtained for transitions at elevated temperatures. The results obtained for  $Mn_3AlC$  by the author ( $\Delta S = 0.15$  cal/g.atom/deg.) are indeed very low and indicate that for accurate results a larger temperature range, and in particular measurements at low temperatures to determine the Debye constant, are required.

The entropy changes observed for each of the anomalies of  $Mn_3ZnC$  ( $\Delta S \approx 0.15$  cal/g.atom/deg.) are similarly very low. The total entropy change for both anomalies should be  $3/2 R \ln 2$  per gram-atom of manganese, if  $J = 1/2$  for the ferromagnetic state. The entropy change for the upper transition from  $-33^\circ C$  to  $100^\circ C$  (for  $T/\theta > 0.70$ ), assuming the theoretical ( $C_M, T$ ) curve for  $J = 1/2$ , is  $(0.41)3/2R$ . Thus the entropy change for the low temperature anomaly is  $3/2 R(0.28) = 0.8$  cal/g.atom/deg. This is of course only a crude estimate, since local ordering above the ferromagnetic Curie temperature, as well as other factors, were not taken into consideration. Nevertheless, it is apparent that the experimental results for  $Mn_3ZnC$  are not of the correct order of magnitude.

It is feasible that accurate specific heat measurements over a large temperature range would make possible a precise determination of the entropy change and consequently a verification of the low temperature magnetic structure of  $Mn_3ZnC$ . To do this, a detailed theory of the degree of disorder in the ferrimagnetic and ferromagnetic structures, and the degree of order in the paramagnetic state would be necessary. But difficulties would certainly be encountered in the overlap of the two anomalies, and the rapid rise of the lattice and electronic specific heats in the anomalous region make an accurate separation of the magnetic specific heats doubtful. The object of

the present research in any case was merely to determine the presence of the two anomalies, and the small experimental temperature range permitted no accurate entropy change calculation. However, the determination that transitions from ferrimagnetism to ferromagnetism to paramagnetism occurred is in itself significant.

Calculation of the magnetic anomaly of a ferromagnetic substance is further complicated by the possibility that the drop in the magnetic specific heat at the Curie point may be masked by a sudden increase in the specific heat caused by electronic distribution. This result is produced by the collective electron theory of Stoner.<sup>27</sup> He assumed that ferromagnetism was caused by holes in the 3d band, which was assumed parabolic near the Fermi limit. He also assumed that the exchange energy varied as the square of the relative magnetization (as did Weiss), and that the particles obeyed Fermi-Dirac statistics. Then it was found that at the Curie point a drop in magnetic specific heat of  $\Delta C_M/R = -1.8$  was compensated by a rise in electronic specific heat of  $\Delta C_E/R = 1.2$ , so that the resultant discontinuity was only  $\Delta C/R = -0.6$ . This is not however in agreement with experiment for many ferromagnetic substances. By making the exchange energy also vary with higher powers of the magnetization this difficulty was overcome, and also the magnetization curves were in better agreement with experiment.<sup>28</sup>

c. Theories of exchange interactions:

In order to fully appreciate the phenomena of ferro- and ferrimagnetism, the cause of the Weiss intermolecular field must be considered. Heisenberg<sup>29</sup> originally explained it by exchange interaction between electrons of neighbouring atoms in terms of the Heitler-London method of localized atomic wave functions.

Slater<sup>30</sup> extended this theory to apply to ferromagnetic materials. He assumed that a positive exchange integral (and thus ferromagnetism) resulted from exchange between adjacent 3d shells when the ratio of internuclear distance to d shell diameter was larger than a certain value.

Zener,<sup>31</sup> however, stated that d-d coupling always gives a negative exchange integral (producing antiparallel spins), and that ferromagnetism is caused by a positive exchange integral between conduction electrons and incomplete d shells. (In his calculations he used localized atomic wave functions for the incomplete d shell electrons and band wave functions for the outer s electrons). Zener's theory is useful for Heusler alloys and ferrites, but some disagreement with neutron diffraction data has been noted.

Slater<sup>32</sup> has proposed that to overcome difficulties of non-orthogonal wave functions of the Heisenberg method, determinantal wave functions composed of orthogonal energy-band orbitals should be used. If a single determinantal wave function is used, the energy-band or collective electron theory results, which is quite useful for small internuclear distances. However, for complete accuracy all possible linear combinations of possible determinantal wave functions must be made. This however entails an enormous amount of calculations, and makes practical applications difficult.

The difficulty in explaining the presence of ferrimagnetism and antiferromagnetism in terms of exchange energies is more profound. One approach is the consideration of exchange interaction between excited valence states of cations of the same transition element (super exchange).<sup>33</sup> The completely general theory of Slater<sup>32</sup> is also certainly theoretically applicable to this problem.

## 2. Conclusions.

### a. The Calorimeter.

An ~~aneroid~~ adiabatic calorimeter was constructed in order to measure specific heat anomalies of certain magnetic alloys between  $-150$  and  $150^{\circ}\text{C}$ . The difficulties of accurate temperature and heat input measurement were overcome by using a strain-free platinum resistance thermometer-heater. The accuracy of the calorimeter was  $0.5\%$ ; the use of an accurate bridge for resistance measurements would increase it to  $0.2\%$ .

### b. Specific Heat Measurements.

Specific heat curves were successfully measured for the alloys  $\text{Mn}_3\text{AlC}$  and  $\text{Mn}_3\text{ZnC}$ . The expected second order specific heat anomaly was observed for the former at its ferromagnetic Curie point,  $-10^{\circ}\text{C}$ . The presence of two second order anomalies on the specific heat curve of  $\text{Mn}_3\text{ZnC}$  supported the idea of a complex magnetic behaviour for the alloy: it is ferrimagnetic below  $-35^{\circ}\text{C}$ , ferromagnetic between  $-35$  and  $65^{\circ}\text{C}$  and paramagnetic above  $65^{\circ}\text{C}$ .

The observed anomalies were qualitatively in agreement with the theory of Weiss. Accurate separation of the magnetic specific heats, which would make a quantitative theoretical interpretation of the results feasible, was impossible because of the limitations of the experimental data.

VI. APPENDICESAppendix ICalculation of Effective Magnetization of Mn Atoms.

The alloy  $\text{Mn}_{60}\text{Al}_{20}\text{C}_{20}$  has a magnetization of  $\mu_1 = 1.22\mu_B$  per Mn atom. The alloy  $\text{Mn}_{64}\text{Al}_{16}\text{C}_{20}$ , in which 4 atomic percent of Mn atoms have replaced Al atoms, has an average magnetization  $\mu_c = 0.89\mu_B$  per Mn atom. The decrease is assumed caused by the extra c (=4) atomic percent Mn atoms, with a magnetization of  $\mu_2$ , which is assumed independent of  $\mu_1$ .

then

$$(c + 60)\mu_c = 60\mu_1 + c\mu_2$$

$$\mu_2 = \mu_c + 60(\mu_c - \mu_1)/c$$

$$\mu_2 = 0.89 + 60(0.89 - 1.22)/4$$

$$\mu_2 = -4.06\mu_B$$

Thus, if replacing Al atoms by Mn atoms in the alloy  $\text{Mn}_3\text{AlC}$  does not change the magnetization of those Mn atoms already present, the resulting decrease in magnetization is explained by assuming the extra Mn atoms have a magnetization of  $-4\mu_B$ .

## Appendix II

### Antiparallel Spin Systems

#### 1. General Theory of Antiparallel Spin Systems<sup>18</sup>:

A ferrimagnetic or antiferromagnetic substance consists of two or more sublattices with antiparallel spin systems (with opposing magnetization vectors). Consider two sublattices, A and B, and let the fractional volume of A and B atoms be  $\lambda$  and  $\mu$  ( $\lambda + \mu = 1$ ). The magnetizations of the sublattice atoms are  $\bar{I}_A$  and  $\bar{I}_B$ , so that the resultant magnetization is

$$\bar{I} = \lambda \bar{I}_A + \mu \bar{I}_B \quad (1)$$

The internal Weiss molecular fields,  $\bar{H}_A$  and  $\bar{H}_B$ , acting on A and B atoms depend on  $\bar{I}_A$  and  $\bar{I}_B$ :

$$\bar{H}_A = N(\alpha \lambda \bar{I}_A - \mu \bar{I}_B) \quad (2)$$

$$\bar{H}_B = N(B \mu \bar{I}_B - \lambda \bar{I}_A) \quad (3)$$

thus

$$H_A = N(\alpha \lambda I_A + \mu I_B) = |\bar{H}_A| \quad (4)$$

$$H_B = N(B \mu I_B + \lambda I_A) \quad (5)$$

since  $\bar{I}_A$  is in the opposite direction to  $\bar{I}_B$ .  $N$  is the Weiss intermolecular field constant and  $\alpha$  and  $B$  represent the strength of the effect the sublattices have on their own molecular fields.

And, according to Curie, for paramagnetism:

$$\bar{I}_A = \frac{C}{T} (\bar{H} + \bar{H}_A) \quad (6)$$

$$\text{and } \bar{I}_B = \frac{C}{T} (\bar{H} + \bar{H}_B) \quad (7)$$

$C$  is the Curie constant and  $\bar{H}$  is the applied field. The effective field,

$$\bar{H}_e = \bar{H} + \bar{H}_A \text{ or } \bar{H} + \bar{H}_B$$

Solving equations (1), (2), (3), (6), and (7):

$$\frac{H}{I} = \frac{1}{\chi} = \frac{T}{C} + \frac{1}{\chi_0} - \frac{\sigma}{T - \Theta} \quad (8)$$

where  $\chi$  = susceptibility,

$$\chi_0 = \frac{C}{\lambda + \Theta}$$

$$\sigma = \frac{-\nu - \Theta(\lambda + \Theta)}{C}$$

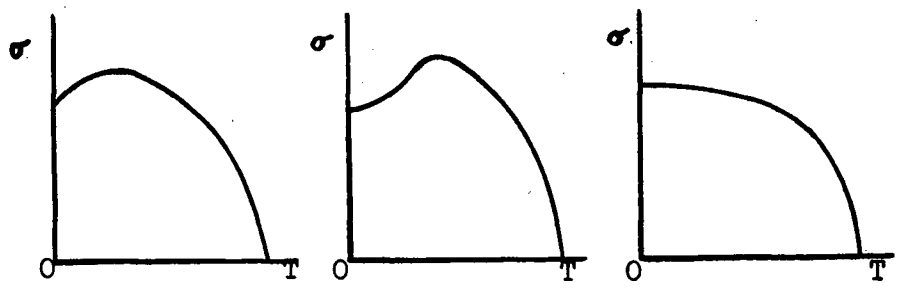
$$\Theta = NC\mu\lambda(2 + \alpha + B)$$

and  $\lambda = -NC(\mu B + \lambda\alpha)$

$$\nu = N^2C^2\mu\lambda(\alpha B - 1)$$

This is the equation for the paramagnetic behaviour of a ferrimagnetic substance. It is a hyperbola with curvature concave to the temperature axis.

Néel predicted several types of variation of saturation magnetization with temperature for ferrimagnetic substances. Three of these are as shown:



## 2. Energy of Magnetization of Antiparallel Spin Systems:

The absolute value of the effective field acting on A or B atoms is:

$$H_e \approx H_A \text{ or } H_B$$

Therefore the energy of magnetization per unit mass,

$$\begin{aligned}
 U &= -\frac{\lambda}{\rho} \int_0^{I_A} H_A dI_A - \frac{\mu}{\rho} \int_0^{I_B} H_B dI_B \\
 &= -\frac{N}{\rho} \left[ \lambda \int_0^{I_A} \alpha \lambda I_A dI_A + \lambda \int_0^{I_A} \mu I_B dI_A \right. \\
 &\quad \left. + \mu \int_0^{I_B} \mu I_B dI_B + \mu \int_0^{I_B} \lambda I_A dI_B \right]
 \end{aligned}$$

from equations (4) and (5),

For an antiferromagnetic substance,

$$\lambda I_A = \mu I_B, \quad \text{since } I = 0,$$

$$\text{and } \alpha = B, \quad \text{since } H_A = H_B$$

$$\text{thus } U = -\frac{N}{\rho} \frac{I_A^2}{2} \lambda^2 (\alpha + B + 2)$$

$$U = -\frac{N}{\rho} I_A^2 \lambda^2 (\alpha + 1)$$

This value is the same as that of a ferromagnetic substance of magnetization  $I_A$  (see equation (4) of I, 1) if  $2\lambda^2(\alpha + 1) = 1$ . This would be the case if  $\alpha = 1$  and  $\lambda = \frac{1}{2}$ , which would occur for a simple lattice in which A and B atoms were identical except for antiparallel spins, and they occupied equivalent lattice sites.

Assuming the ferrimagnetic postulated behaviour of Mn-Al-C alloys, the magnetization energy can be calculated for an alloy  $Mn_{64}Al_{16}C_{20}$ , in which four out of every 64 Mn 'B' atoms have a spin of -4, antiparallel to the spin of 1.2 of the other 60 'A' atoms:

$$I_B = \frac{4}{1.2} I_A = \frac{10}{3} I_A$$

$$\mu = \frac{4\lambda}{60} = \frac{\lambda}{15}$$

$$\text{therefore } \mu I_B = \frac{2}{9} \lambda I_A$$

thus

$$\begin{aligned}
 U' &= -\frac{N}{\rho} \frac{I_A^2}{2} \left[ \alpha \lambda^2 + \frac{2}{9} \lambda^2 + \frac{4}{81} B \lambda^2 + \frac{2}{9} \lambda^2 \right] \\
 &= -\frac{N}{\rho} \frac{I_A^2}{2} \frac{\lambda^2}{81} [81\alpha + 4B + 36]
 \end{aligned}$$

If  $\alpha = B = 1$ ,  $U' \approx -\frac{2}{4} \frac{N}{\rho} I_A^2 \lambda^2$

Since  $Mn_3AlC$  is ferromagnetic, then its magnetization energy,

$$U'' = -\frac{N\rho\sigma^2}{2} \quad (\text{equation (4) of Section I, 1}).$$

But  $\rho\sigma = \lambda I_A$ , since the magnetization of the Mn atoms in  $Mn_3AlC$  is assumed equal to  $I_A$ , the magnetization of the Mn atoms of the A sublattice in  $Mn_{64}Al_{16}C_{20}$ .  $\lambda$  is the same for both alloys, because the Mn and Al atoms have about the same diameter.

Thus,

$$U'' = -\frac{N\lambda^2 I_A^2}{2\rho} = \frac{2}{3} U'$$

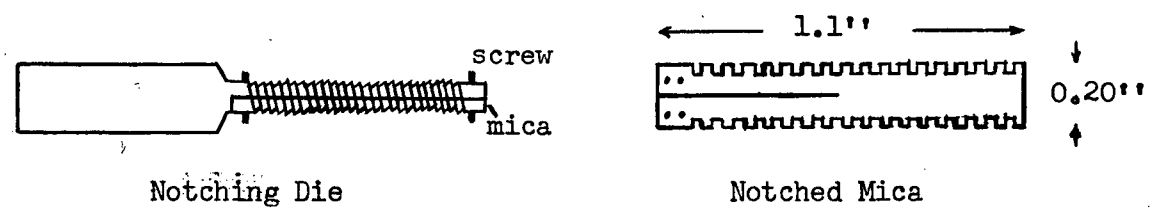
The total magnetization energy,  $U''$ , is only  $\frac{2}{3}$  as great as for the ferrimagnetic state (if N is the same in both cases).

Appendix III

Assembly of the Thermometer Mica Cross

The mica cross was assembled as follows: mica sheet 0.003 inch thick was clamped between smooth steel bars and cut with a razor blade into 0.20 by 1.1 inch pieces. Two pieces were slotted half way so that they could fit together lengthwise at right angles, forming a cross. A die formed from four small steel bars was used for the slotting. Small holes were drilled through the mica at one end to permit anchoring of the leads.

The pieces of mica were notched along each side by placing them in a grooved die and cutting out the mica with 0.008 in. piano wire held in a metal bow. The die was made by machining 0.30 in. of 3/8" brass rod down to 0.2 in. diameter and then threading at 29 per inch. The threaded part of the rod was then split by cutting lengthwise. One half of the split rod was removed and attached to the other half with screws at either end, so that the mica could be held firmly between the halves.



The mandrel used to hold the assembled mica cross was constructed by soldering together four bars of 3/16 inch brass and machining down to a 0.150

diameter rod. The platinum helix was wound non-inductively on the mica cross and the two leads were fastened through the holes drilled for the purpose.

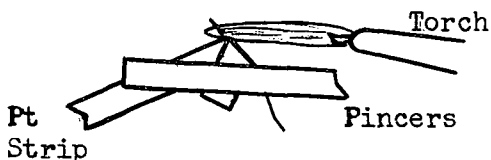
Appendix IV

Construction of the Thermometer Pyrex Case

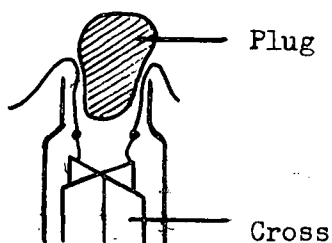
The thermometer case was made by first drawing out 1 inch diameter pyrex glass tubing in a broad oxygen-gas flame to about 0.28 inch diameter, in order to obtain thin-walled tubing. This tubing was necked slightly at the end where the leads were to emerge.

In order to make a leak-tight seal of the platinum leads through pyrex glass, a special technique was used.<sup>14</sup> Platinum strips, rolled from 0.010 inch wire to less than 0.001 inch thick, were used for the seal. Because of their thinness and the resulting feathered edges, these strips give a vacuum-tight seal through pyrex.

To fuse a strip to the 0.003 inch platinum thermometer wire, the strip was folded over the end of the wire, and the wire was fused to the corner of the fold with a small oxy-gas flame. A micro-burner is not needed for this flame if pincers are used, as shown, to prevent melting of the fine platinum wire.



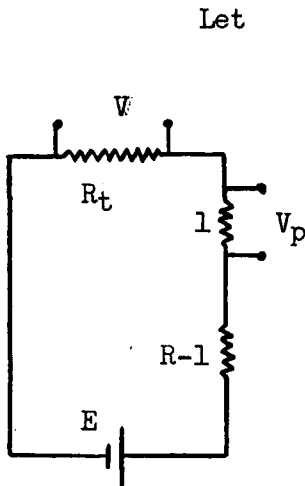
After the platinum strips were fused to the leads, the thermometer coil was pushed into the pyrex tubing and the two strips were bent over the necked end. The strips were cleaned with acetone, and fire polished at near the



melting point with a gas flame. A plug, made from pyrex rod, was placed in the tube end, and fused with a soft flame to the tube and about 1/8 inch of the platinum strips. The seal was cooled slowly in a yellow flame to remove strains. The seal was tested in a vacuum system, after being immersed in liquid oxygen.

Appendix V

Calculation of Power Change for the Thermometer-Heater (see Figure 8b)



Let

$R_{t_0}$  = the initial heater resistance,

$R_{t_1} = R_{t_0} + \Delta R_t$  = the final heater resistance,

$E$  = the constant voltage supply,

$R$  = the resistance of the circuit minus heater resistance,

$V_0, V_1$  = initial, final voltages across heater.

The initial current,  $I_0 = \frac{E}{R + R_{t_0}}$

The final current,  $I_1 = \frac{E}{R + R_{t_1}}$

$V_0 = I_0 R_{t_0}$

$V_1 = I_1 R_{t_1} = \frac{E R_{t_1}}{R + R_{t_1}}$

$V_0 I_0 = R_{t_0} I_0^2 = P_0$ , the initial power through heater;

the final power,  $P_1 = V_1 I_1 = \frac{E^2 R_{t_1}}{(R + R_{t_1})^2} = I_0^2 R_{t_1} \left( \frac{R + R_{t_0}}{R + R_{t_1}} \right)^2$

$\frac{P_1}{P_0} = \frac{R_{t_1}}{R_{t_0}} \left( \frac{R + R_{t_0}}{R + R_{t_1}} \right)^2$

For  $R \ll R_t$ , as with the 100 ohm thermometer (Figure 8a):

$\frac{P_1}{P_0} \approx \frac{R_{t_0}}{R_{t_1}} \approx \frac{25}{26}$  for a 10°C temperature rise.

For  $R = R_{t_0}$ , as with the 20 ohm thermometer (Fig. 8b):

$$\frac{P_1}{P_0} = \frac{R_{t_1}}{R_{t_0}} \frac{4 R_{t_0}^2}{(R_{t_0} + R_{t_1})^2} = \frac{4 R_{t_0} (R_{t_0} + \Delta R_t)}{(2 R_{t_0} + \Delta R_t)^2}$$

For a 10°C temperature rise,

$$\Delta R_t \approx .04 R_{t_0}$$

$$\text{therefore } \frac{P_1}{P_0} = \frac{4 R_{t_0} 26 R_{t_0}}{25(2 R_{t_0} + .04 R_{t_0})^2} = \frac{4 \times 26}{(2.04)^2 \times 25}$$

$$\frac{P_1}{P_0} = \frac{4160}{4162} = 0.9995$$

The percent difference is 0.05%

$$\text{for } \frac{P_1}{P_0} = 1,$$

$$R = 1.02 R_{t_0} \quad \text{if } \Delta R_t = 0.04 R_{t_0}$$

That is, for no power change, R must be half way between  $R_{t_0}$  and  $R_{t_1}$ .

Appendix VI

Equivalence of Resistance-Temperature Equations for a Platinum Resistance Thermometer.

The general equation connecting resistance and temperature for a platinum resistance thermometer is:

$$R_t = R_0(1 + At + Bt^2)$$

for  $0 < t < 630^\circ\text{C}$ .

$$\begin{aligned} \text{thus } t - \frac{R_t - R_0}{R_{100} - R_0} 100 &= t - \frac{At + Bt^2}{100A + 100^2B} 100 \\ &= \frac{100Bt - Bt^2}{A + 100B} \end{aligned}$$

$$\begin{aligned} \text{therefore } t - \frac{R_t - R_0}{R_{100} - R_0} 100 &= \frac{100^2 B}{A + 100B} \left[ \frac{t}{100} - \left( \frac{t}{100} \right)^2 \right] \\ &= -\delta \left[ \frac{t}{100} - \left( \frac{t}{100} \right)^2 \right] \end{aligned}$$

according to Callendar's equation.

$$\text{therefore } \delta = - \frac{100^2 B}{A + 100B}$$

$\approx 1.5$  for pure platinum

For temperatures between  $-183$  and  $0^\circ\text{C}$ ,

$$R_t = R_0 \left[ 1 + At + Bt^2 + C(t - 100)t^3 \right]$$

$$\begin{aligned} t - \frac{R_t - R_0}{R_{100} - R_0} 100 &= t - \frac{At + Bt^2 + C(t - 100)t^3}{100A + 100^2 B} 100 \\ &= \frac{100Bt - Bt^2 - C(t - 100)t^3}{A + 100B} \end{aligned}$$

$$t - \frac{R_t - R_0}{R_{100} - R_0} 100 = - \frac{100^2 B}{A + 100B} \left[ \left( \frac{t}{100} \right)^2 - \frac{t}{100} \right] - \frac{C}{A + 100B} (t - 100)t^3$$

The last term may be written:

$$+ D(t - 100)t^3$$

where  $D = - \frac{C}{A + 100B}$

Thus in Callendar form, the equation is:

$$t = \frac{R_t - R_o}{R_{100} - R_o} 100 + \delta \left[ (0.01t)^2 - 0.01t \right] + D(t - 100)t^3$$

Appendix VII

Error in Temperature Interval Caused by Error in Calibration of Resistance Thermometer.

Above 0°C, the temperature of a resistance thermometer is:

$$t = \frac{R_t - R_0}{R_{100} - R_0} 100 + \delta [ (.01t)^2 - .01t ]$$

The interval between two temperatures,

$$\begin{aligned} t - t_1 = \Delta t &= \frac{R_t - R_{t_1}}{R_{100} - R_0} 100 + \delta [ (.01t)^2 - (.01t_1)^2 + .01t_1 - .01t ] \\ &= \frac{\Delta R_t}{R_{100} - R_0} 100 + \delta [ (.01)^2 (t + t_1) \Delta t - .01 \Delta t ] \end{aligned}$$

$$\begin{aligned} \text{therefore } \Delta t &= \frac{\Delta R_t}{R_{100} - R_0} \frac{100}{1 - \delta [ (.01)^2 (t + t_1) - .01 ]} \\ &= \frac{\Delta R_t}{R_{100} - R_0} \left\{ 1 + \delta [ (.01)^2 (t + t_1) - .01 ] \right. \\ &\quad \left. + \delta^2 [ (.01)^2 (t + t_1) - .01 ]^2 + \dots \right\} \end{aligned}$$

for  $0 < t < 100$ ,

$$\delta^2 [ (.01)^2 (t + t_1) - .01 ]^2 < (.015)^2 < .0004$$

so that this term is negligible in comparison with unity.

$$\text{therefore } \Delta t = \frac{\Delta R_t}{R_{100} - R_0} \left\{ 1 + \delta [ (.01)^2 (t + t_1) - .01 ] \right\}$$

With a different calibration,

$$\Delta t' = \frac{\Delta R_t}{(R_{100} - R_0)'} \left\{ 1 + \delta' [ (.01)^2 (t + t_1)' - .01 ] \right\}$$

Thus the error in temperature interval,

$$(1) \Delta t - \Delta t' = \Delta R_t \left\{ \frac{100}{R_{100} - R_0} - \frac{100}{(R_{100} - R_0)'} + \frac{100\delta[-]}{R_{100} - R_0} - \frac{100\delta'[-]'}{(R_{100} - R_0)'} \right\}$$

If  $\delta = \delta'$  and  $t = 100^\circ\text{C}$ .

$$\begin{aligned} \Delta t - \Delta t' &= \Delta R_t 100 \left\{ \frac{1}{R_{100} - R_0} - \frac{1}{(R_{100} - R_0)'} + \frac{0.01\delta}{R_{100} - R_0} - \frac{0.01\delta}{(R_{100} - R_0)'} \right\} \\ &= \Delta R_t 102 \left\{ \frac{1}{R_{100} - R_0} - \frac{1}{(R_{100} - R_0)'} \right\}, \end{aligned}$$

if  $\delta = 2$ .

$R_{100} - R_0 \approx 0.4 R_0$  for platinum ;

put  $(R_{100} - R_0)' = (0.4 + \epsilon)R_0$ .

In a  $10^\circ\text{C}$ . temperature interval,  $\Delta R_t \approx .04 R_0$

$$\begin{aligned} \text{therefore } \Delta t - \Delta t' &= .04 R_0 102 \left\{ \frac{1}{0.4 R_0} - \frac{1}{(0.4 + \epsilon)R_0} \right\} \\ &= 4.08 \frac{\epsilon}{0.4(0.4 + \epsilon)} \end{aligned}$$

If  $\epsilon = 0.002$  (eg. if  $R_{100} - R_0$  changed by 0.2 ohms for the 100 ohm thermometer: a very large change),

$$\Delta t - \Delta t' = \frac{4.08 \times 0.002}{0.4 \times 0.402} = 0.051^\circ\text{C}.$$

Thus the error in temperature interval would be:

$$\frac{\Delta t - \Delta t'}{\Delta t} 100 = \frac{0.05}{10} 100 = 0.5\%$$

This error is considerably less than the error in temperature caused by a change in  $R_{100} - R_0$  of  $\epsilon R_0$ : if  $R_0$  remains the same,  $R_{100}$  changes by  $\epsilon R_0$ . Thus the temperature error would be  $\frac{\epsilon R_0}{0.4 R_0} 100 = 0.5^\circ\text{C}$  at  $100^\circ\text{C}$  for  $\epsilon = 0.002$ .

The error in temperature interval caused by the change in calibration observed for the commercial thermometer (see Section III, 1d), for

$$\Delta R_t = 4.00 \text{ at } 100^\circ\text{C, was}$$

$$\begin{aligned} \Delta t - \Delta t' &= 4.00(2.5786 - 2.5740 + 2.5786 \times 2.17 \times .01 - 2.5740 \times 1.47 \times .0101) \\ &= 0.09^\circ\text{C} \quad (\text{using Equation 1}) \end{aligned}$$

Since  $\Delta t \approx 10^\circ$ , the error was 0.9%. This error would be less for any temperature between 0 and  $100^\circ\text{C}$ .

BIBLIOGRAPHY

1. F. Seitz, 'The Modern Theory of Solids', McGraw-Hill, 1940.
2. J. Roberts, 'Heat and Thermodynamics', Blackie.
3. E. Lapp, Ann. Physique 12, 442 (1929).
4. R. Butters, and H. Myers, Phil. Mag. 46, 895 (1955).
5. R. Butters, and H. Myers, Phil. Mag. 46, 132 (1955).
6. B. Brockhouse and H. Myers, Canadian J. Phys. 35, 313 (1957)
7. W. White, 'The Modern Calorimeter', The Chemical Catalog Co.
8. E. Griffiths, 'Methods of Measuring Temperature', Griffon 1947.
9. R. Weber, 'Temperature Measurement and Control', Blakiston 1941.
10. Southard, Brickwedde, J. Am. Chem. Soc. 55, 4378.
11. A. Reddoch, Master of Science Thesis, Queen's University, Aug. 1954.
12. J. Southard and D. Andrews, J. Franklin Inst. 209, 349 (1930).
13. C. Meyers, Bureau of Standards J. Research 9, 807 (1932).
14. N. Rasor, Rev. Sci. Instr. 25, No. 4, 316 (1954).
15. D. Ginnings, and G. Furukawa, J. Am. Chem. Soc. 75, 522 (1953).
16. K. Grew, P.R.S. 145, 509 (1934).
17. R. Bozorth, 'Ferromagnetism', Van Nostrand, 1951.
18. L. Néel, Ann. Phys. 3, 137 (1948).

19. P. Weiss, J. Phys. (4) 6, 661, (1907).
20. J. Went, Physica, 17, 98, 596 (1951).
21. S. Friedberg, Physica 18, 714 (1952).
22. J. Daniels, F. Robinson, Phil. Mag. (7), 44, 630 (1953).
23. E. Stoner, Phil. Mag. (7), 22, 81 (1936).
24. N. Mott, H. Jones, 'Theory of Properties of Metals and Alloys', Clarendon Press 1936.
25. J. Awberry, E. Griffiths, Proc. Roy. Soc. (London), 174A, 1.
26. P. Kasteleijn, J. VanKranendonk, Physica 22, 317
27. E. Stoner, Proc. Roy. Soc, (London) A169, 339 (1939).
28. E. Wohlfarth, Rev. Mod. Phys. 25, 211 (1953).
29. W. Heisenberg, Z. Physik 49, 619 (1928).
30. J. Slater, Phys. Rev. 36, 57 (1930).
31. C. Zener, Phys. Rev. 81, 440 (1951); 83, 299 (1951).
32. J. Slater, Rev. Mod. Phys. 25, 199 (1953).
33. J. Van Vleck, Grenoble Conference, 114 (1951).